We are IntechOpen, the world's leading publisher of Open Access books Built by scientists, for scientists

4,800
Open access books available

122,000
International authors and editors

135M
Downloads

Our authors are among the

154
Countries delivered to

TOP 1%
most cited scientists

12.2%
Contributors from top 500 universities

CLARIVATE ANALYTICS BOOK CITATION INDEX INDEXED

WEB OF SCIENCE™

Selection of our books indexed in the Book Citation Index in Web of Science™ Core Collection (BKCI)

Interested in publishing with us?
Contact book.department@intechopen.com

Numbers displayed above are based on latest data collected.
For more information visit www.intechopen.com

10

Translational and Rotational Motions for TFSA-Based Ionic Liquids Studied by NMR Spectroscopy

Kikuko Hayamizu
National Institute of Advanced Industrial Science and Technology
AIST Tsukuba Central 2, Tsukuba, Ibaraki
Japan

1. Introduction

Solution-state NMR spectroscopy is an important method to study chemical structures, intramolecular local motions and translational and rotational motions of a whole molecule. NMR parameters of the solution-state NMR are chemical shift, spin-spin coupling constant, spectral pattern including line width, spin-lattice relaxation time (T_1) and spin-spin relaxation time (T_2). The assignment of the spectral signals is the starting task for advanced studies. Various two-dimensional (2D) NMR techniques can help to make assignments for complex compounds. Additionally, 2D-NMR techniques afford information on the intermolecular interactions or molecular diffusion. Generally, chemical structures of ionic liquids (IL) are not complex and the NMR spectra can be assigned easily using general rules. Once the assignment is fixed, we can obtain the precise data for the individual species for ILs. Multinuclear NMR techniques can be applied to magnetic active nuclei, and the nuclei relating to ILs are ^{1}H, ^{2}H, ^{7}Li, ^{11}B, ^{13}C, ^{19}F, ^{31}P and others. In addition to general NMR spectra, self-diffusion coefficient (D) of each ion can be measured by the pulse-gradient spin-echo (PGSE) NMR method. The D's of the individual ions in ILs are important to understand translational motion of ions.

In this chapter, NMR studies for four ILs having a common anion bis(fluoromethylsulfonyl)amine (TFSA) will be described. The cations are N-ethyl-N-methylimidazolium (EMIm), N,2-dimethyl-N-propylimidazolium (DMPIm), N-methyl-N-propylpyrrolidinium (P13), and N,N-diethyl-N-methyl-N-(2-methoxylethyl)ammonium (DEME). These ILs are important candidates to use as electrolytes in various batteries or cells. The basic properties of molecular weight (MW), viscosity (η) and cation and TFSA diffusion coefficients (D_{cation} and D_{TFSA}) measured at 30°C are given in Table 1 for the four ILs. The experimental data have been published in our previous papers for individual ILs.[1-4] In the present chapter, the individual experimental data for the four ILs are plotted on a sheet to clarify the cation properties. In addition, newly derived plots of D_{cation} versus correlation times of molecular motion are included. The chemical structures of the ions are shown.

To study the translational and rotational motions of ILs by NMR spectroscopy, the D's of the individual ions and the T_1's of the individual protons are important parameters in the

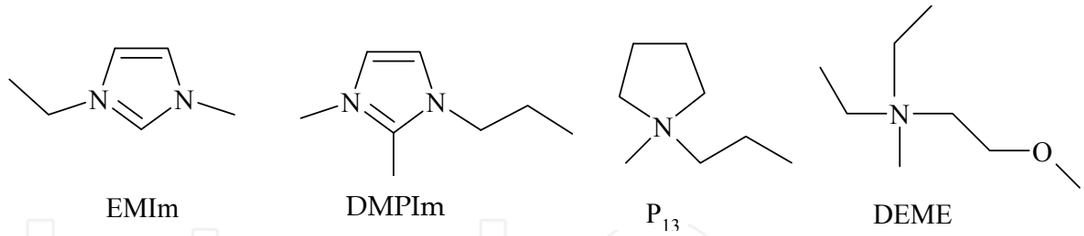

IL	MW	Viscosity η mPas	D_{cation} m^2s^{-1}	D_{TFSA} m^2s^{-1}
EMIm-TFSA	111.2 + 280.1	27.8	6.6×10^{-11}	3.9×10^{-11}
DMPIm-TFSA	139.2 + 280.1	74.8	2.2×10^{-11}	1.5×10^{-11}
P_{13}-TFSA	128.2 + 280.1	49.8	2.9×10^{-11}	2.2×10^{-11}
DEME-TFSA	146.3 + 280.1	56.6	2.3×10^{-11}	2.0×10^{-11}

Table 1. Molecular weight, viscosity and diffusion coefficients of the four ILs at 30 °C.

temperature range for which ILs are in liquid state. Solution-state NMR affords information on molecular motions for liquids or mobile species which behave like liquids. In this chapter, the properties of the ILs in the liquid states will be described, where the spectral lines are sharp enough to measure individual peaks in the solution-mode NMR. The temperature-dependent D values were measured for the cations (D_{cation}) by ^{1}H resonance and the anion of TFSA (D_{TFSA}) by ^{19}F resonance using the PGSE NMR method. Arrhenius plots of ^{1}H T_1 for the cations exhibited T_1 minimum in the temperature range in the liquid state, and the correlation time τ_c(cation) were evaluated for the same temperature range. The molecular motion of a whole molecule of the cations can be assigned to a phenomenon of the T_1 minimum and the timescale estimated was 1~500 ps depending on the temperature. The motion which gives the minimum in the ^{1}H T_1 Arrhenius plots is assumed to be a librational flip rather than an all over reorientational motion of a whole molecule. The τ_c(cation) is related to viscosity and D_{cation}. Since Arrhenius plots of the ^{19}F T_1 did not show a T_1 minimum, the correlation times including internal rotations of CF_3 could not be calculated but also related to the viscosity of the ILs.

In this chapter, complex dynamic properties of the four ILs will be discussed based on the experimental data such as D_{TFSA}, D_{cation}, τ_c(cation), bulk viscosity, ionic conductivity and density in the temperature range from 253 to 353 K or above freezing, while the data of the viscosity and density were measured between 283 and 353 K. Since ILs are in wide variety of structures and rich in properties and applications, the description in this chapter is limited for the four ILs.

2. Measurements of diffusion coefficients by NMR

It is very popular to obtain positional information using nuclear magnetic resonance, so called NMR imaging including medical MRI. In addition of a large coil to produce static magnetic field (presently super-conductive magnet (SCM)), small three-dimensional coils are placed in an NMR probe to produce pulse field gradient (PFG). The diffusion measurement for liquids is based on the same principle, where coils are wound on a NMR probe to produce PFG to the direction of the magnetic field of the SCM. In a special case, if three-dimensional coils were placed, it is possible to measure diffusion coefficients along x,

y, z-directions in an anisotropic circumstance. Application of the PFG is controlled by a pulse sequence in Fig. 1 for (a) the modified Hahn echo (PGSE) and (b) stimulated echo (STE) pulse sequences, and the latter is valid to measure species having short T_2.[5] The two most commonly used pulse sequences in Fig. 1 are important to measure the D's of ILs. Generally, the D's of viscous ILs are smaller compared with solutions prepared by organic and aqueous solvents and thus require larger PFG's to obtain sufficient echo attenuation for accurate D data in ILs at least up to 15 T/m depending on temperature. Generally, a high PFG probe is necessary for the studies on translational diffusion of ILs.

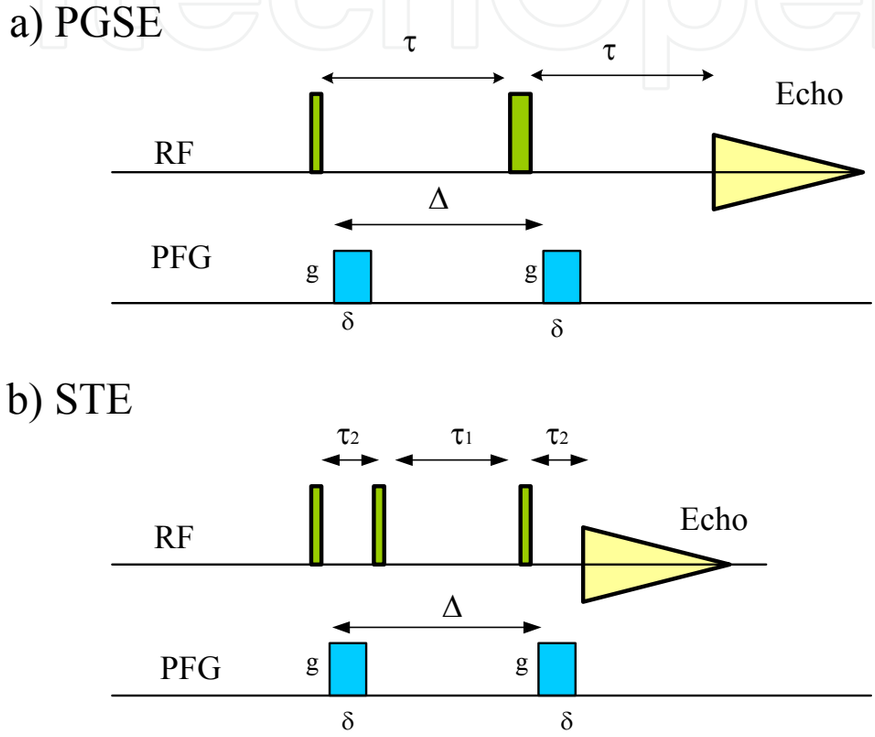

Fig. 1. (a) PGSE and (b) STE pulse sequences used to measure the self-diffusion coefficient (D). The τ's are the intervals of RF pulses, g is the strength of PFG for duration δ, and Δ is the interval between the leading edges of the gradient pulses.

Positional information is acquired in phases of the NMR signals, and basically two equivalent PFG's are applied to the sample. The first PFG pulse can put a mark in the initial position of a target molecule and the second PFG pulse detects the change of the position during the time interval Δ. Originally, Hahn echo sequence (90°-τ-180°-τ-Acq) was proposed to T_2 measurements. The modified Hahn spin-echo (SE) was proposed to incorporate two PFG's.[6] For nuclei having shorter T_2, the stimulated echo (STE) (90°-τ_2-90°-τ_1-90°-τ_2-Acq) was introduced, where τ_2 is related to T_2 process and τ_1 is governed by T_1 process.[7] PGSE data obtained using either pulse sequence can be analyzed by the Stejskal and Tanner equation (1).[6]

$$E = \exp(-\gamma^2\delta^2 g^2 D(\Delta - \frac{\delta}{3})), \quad (1)$$

where γ is the gyromagnetic ratio, g is the strength of the PFG of duration δ, and Δ is the interval between the leading edges of the gradient pulses.
The basic assumptions in the setup of NMR diffusion measurements to be analyzed by the Stejskal and Tanner equation are: (1) all the species must be in a homogeneous external magnetic field to prevent signal attenuation from background magnetic field gradients. The magnitude of the background field gradient can be estimated by the line width of signals. (2) The sample must be placed in the constant region of the PFG, and (3) the RF field must be homogeneous to produce accurate 90° and 180° pulses over the whole sample. In particular, condition (2) is important to achieve accurate measurement for viscous ILs since the requisite large PFG's with constant profile must be generated over limited volume. If the sample conditions were not proper, the measurements may include artifacts. Usually, RF pulse width is in μs order and δ and Δ are in ms order. The PFG magnitude is determined by g × δ where g is larger than approximately 2 T/m for ILs and the largest δ is less than 4 ms to prevent the decay of NMR signal during the PFG application. Eq. (1) implies that the PFG pulse is homogeneous and the decay of the echo signal corresponds to the movement of molecules whose positions are marked by the first PFG pulse and detected by the second PFG pulse. Thus the sample volume must be confined in the PFG coil. Cares are necessary to the external perturbation like convection effect induced by thermal inhomogeneity within the sample, particularly in high temperatures. When the PGSE measuring conditions are adequately prepared to obtain an accurate self-diffusion coefficient, the value becomes a physical constant at a certain temperature. As an example, the attenuation of echo signals following Eq. (1) are shown in Fig. 2 for ^{19}F resonance of TFSA in EMImTFSA measured at 30 °C.

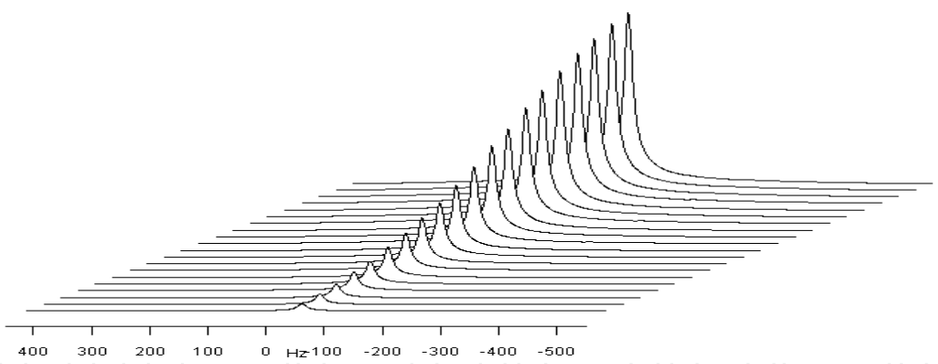

Fig. 2. The attenuation of ^{19}F echo signals of TFSA in EMImTFSA at 30 °C. Δ = 50 ms, g = 2.56 T/m and δ changed from 0.1 to 2 ms (20 points). The effective PFG is determined by g × δ. Following to Eq. (1), the gradient (D) obtained by the plot of ln(E) (E=echo amplitude) versus $-\gamma^2\delta^2 g^2(\Delta - \delta/3)$ was 3.80 ± 0.02 × 10^{-11}m^{2}s^{-1}.

Since the PGSE method measures the movement of the center of gravity of a molecule under study, all the nuclei in a molecule should have the same diffusion coefficient, for example, ^{19}F and ^{11}B resonances of the anion BF_4 in EMIm-BF_4 give the same values of D_{BF4} under suitable measuring conditions. Also, in homogeneous liquids the D values should be independent of Δ, if the experimental conditions are set properly. However, as described later, many ILs having large viscosity behave differently from usual isotropic homogeneous solutions in the diffusion measurements.

3. Spin-lattice relaxation time T_1 for ILs

The ^{1}H and ^{19}F T_1 data for the present ILs are needed in order to set the PGSE measuring conditions and we found that the Arrhenius plots exhibit a T_1 minimum in the ^{1}H resonance. Generally, Arrhenius plots in ^{1}H T_1 for organic solutions are linear where the T_1 values become longer with the increase of temperature. On the contrary, in the solid-state NMR, organic materials often show ^{1}H T_1 minima. Many studies had been made for the ^{1}H T_1 in the solid-state and widely developed about 30 years ago before the attractive techniques of "high resolution solid-state NMR" were introduced. Recently, the studies on ^{1}H T_1 measurements are seldom reported even in the solid-state NMR. Although ILs are liquids, some protons in ILs show a ^{1}H T_1 minimum in the Arrhenius plots where the classical Bloembergen, Purcell and Pound (BPP) equation[8] can be applied to obtain a physical constant of the correlation time τ_c for a motion of ^{1}H-^{1}H dipoles within a molecule in the liquid state. The BPP equation is given in Eq. (2).

$$\frac{1}{T_1} = C\left(\frac{\tau_c}{1+\omega_0^2\tau_c^2} + \frac{4\tau_c}{1+4\omega_0^2\tau_c^2}\right), \tag{2}$$

where ω_o is the observe frequency (rad s^{-1}), τ_c is the correlation time of the dipole-dipole motions. C in Eq. (2) is written as

$$C = \frac{3}{10}\gamma^4\hbar^2\sum_j \frac{1}{r_j^6}, \tag{3}$$

where r is atomic distance between protons and the summation index j is over all interacting dipoles. The T_1 value measured at a certain temperature is not a physical constant, and depends on the measuring frequency and relaxation mechanisms. Owing to the term in brackets in Eq. (2), the T_1 is minimum when $\omega_o\tau_c = 2\pi\nu_0\tau_c = 0.616$. Nicely, the $\sum\frac{1}{r_j^6}$ term in the constant C in Eq. (3) is not necessary to calculate in order to obtain τ_c. It is known that the internal rotations around the three symmetrical axis of CH_3 and segmental motions of long alkyl chains included in ILs are activated and averaged out in the condensed state. Since the cations of the ILs in this study exhibited the ^{1}H T_1 minima in their Arrhenius plots, the correlation time τ_c, a physical constant for molecular motion, can be evaluated at each temperature. Arrhenius plots of ^{19}F T_1 for the CF_3 of TFSA show that the T_1 values become linearly longer as the increase of the temperature. These phenomena are often observed for molecules in isotropic solution state and defined as the extreme narrowing condition, i.e. $\omega_o\tau_c << 1$ and $1/T_1 \propto \tau_c$ from Eq. (2).

The temperature dependence of ^{13}C T_1 have been studied for 1-butyl-3-methyl hexafluorophospate (BMIm-PF_6),[9-11] 1-methyl-3-nonylimidazolium hexafluorophospate (MNIm-PF_6),[12] 1-ethyl-3-methylimidazolium butanesulfonate (EMIm-BSO_3),[13] 1,2-dimethyl-3-propylimidazolium bis(trifluoromethylsulfonyl)amide (DMPIm-TFSA),[1] BMIm-Br[14] and 1-alkyl-3-methylimidazolium butanesulfonate,[15] and the ^{13}C T_1 minima have been observed. Usually, ^{13}C NMR measurements are performed under ^{1}H decoupling, and the transfer efficiency of the ^{1}H polarization (nuclear Overhauser effect, NOE) differs for individual carbons. Furthermore, the ^{13}C relaxation mechanisms include ^{1}H-^{13}C dipolar

interaction, spin-rotation and ^{13}C chemical shift anisotropy effects and thus great efforts are required to evaluate the correlation time $\tau_c(^{13}C)$. Our Arrhenius plots of the ^{13}C T_1 for DMPIm-TFSA showed the minima, but it was difficult to obtain physical constants. Then in this chapter we will not describe the ^{13}C resonance further more.

4. Experimental procedure

The data in this chapter were collected from our published papers[1-4] and compiled for the discussion. Although the experimental procedures have been written in each paper, the essential parts are summarized here. For NMR diffusion measurements, the samples were placed into a 5-mm NMR microtube (BMS-005J, Shigemi, Tokyo) to a height of 5 mm and sealed with epoxide resin under argon atmosphere to exclude moisture. The small height of the sample is important to prevent convection effects and also to obtain the homogeneity of the PFG. All NMR spectra were measured on a Tecmag Apollo with a 6.35 T wide bore magnet using a multinuclear JEOL PFG probe controlled by a JEOL console. The measurements of various nuclei are possible by tuning the probe for resonance frequencies with keeping the temperature. The gradient strength was calibrated by using H_2O and D_2O (^2H NMR at the frequency 41.5 MHz). The maximum PFG strength is 20 T/m. The T_1 measurements were performed using the inversion recovery (180°-τ-90°-Acq.) sequence. The ^1H and ^{19}F NMR spectra were measured at 270.2 and 254.2 MHz, respectively. ^1H spectra of the four cations and the spectral assignments are shown in Fig. 3.

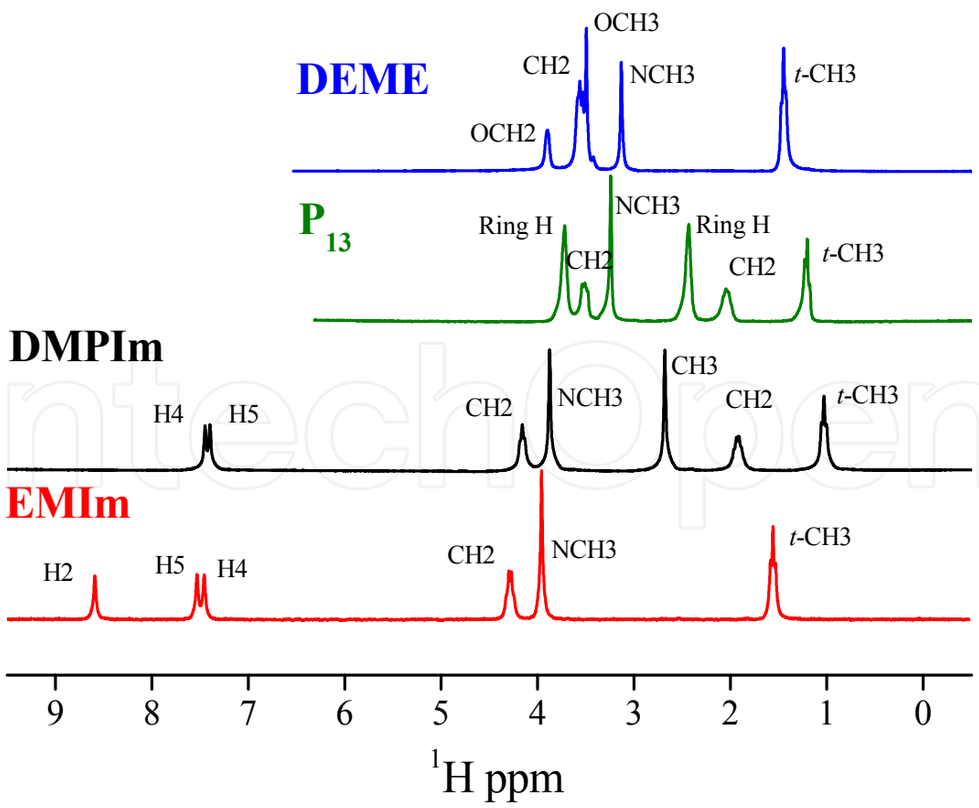

Fig. 3. ^1H spectral patterns of the four cations at 30 °C and the spectral assignments.

Although the line widths of ^{1}H spectra are not very sharp for ILs owing to the high viscosity, the ^{1}H spectra show splitting due to the ^{1}H-^{1}H spin coupling as shown in Fig. 3. The spin-spin coupling J influences the phases of the resonances in the echo signals depending on the J-values. For example, echo signals for resonances with J = 7 Hz are distorted significantly around τ = 23 (= $1/(2\pi J)$), 45 (= $2/(2\pi J)$), 68 (= $3/(2\pi J)$) ms. The J-coupling modulations produce deleterious effects in PGSE experiments such that depending on the choice of τ. There can be large loss in signal-to-noise and distortion of the line-shape. Nevertheless, providing that there is sufficient signal-to-noise, the correct diffusion coefficient can be obtained. For references, the effects of J-evolution on the EMIm echo signals obtained with the PGSE and STE pulse sequences are shown in Fig. 4(b) and 4(c).

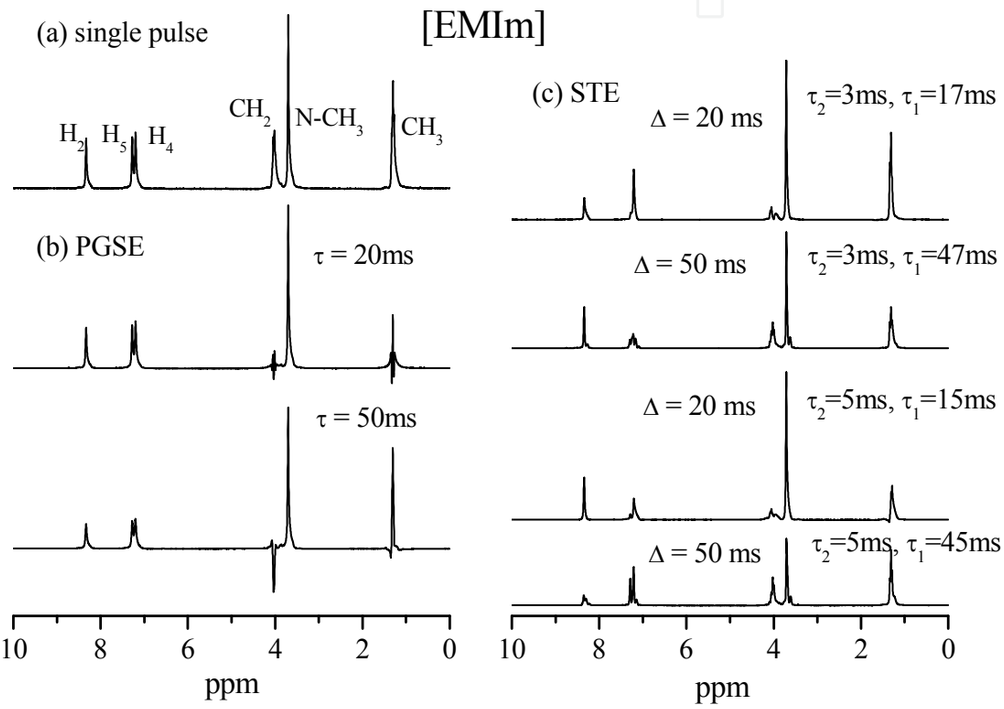

Fig. 4. ^{1}H spectra of EMIm measured with (a) single pulse, (b) Hahn (PGSE) and (c) stimulated echo (STE) sequences. The STE echo signals were measured with small and short PFGs.

Although the ethyl signals are significantly influenced by the J-evolution, the N-CH_3 and imidazolium ring proton signals with negligible spin-spin coupling are almost unchanged and in all cases the evolution effects are insensitive to the presence or absence of the PFGs. The signals obtained with the STE sequence for different delay combinations under short and small PFGs are shown in Fig 4(c). Without PFGs, the J-coupled signals were significantly distorted. For freely diffusing species the values of these three parameters are somewhat arbitrary, if the sufficient echo signal attenuation can be achieved to enable an accurate diffusion measurement as shown in Fig. 2.

The time interval Δ in the pulse sequences shown in Fig. 1 is an important parameter for the diffusion measurements. Practically, long Δ induces the reduction of S/N ratio due to the T_2 effect and T_1 effect in the STE pulse sequence. Also the convection effects may have a chance

to enlarge the diffusion coefficients by the long interval due to the thermal inhomogeneity within a sample. A short Δ requires a large effective PFG. It is important to confirm that the two strong PFG's are equivalent for short Δ.[16] If the pulse duration, δ were too long, the magnetization may decay during the PFG application. The accuracy of short δ values is related to a rectangular shape of the PFG pulse. It is necessary to estimate the accuracy of D values measured by individual PFG probes. We found that the reliable limit of short Δ is 20 ms in our PFG probe.

The Δ-dependence of D for species in structurally heterogeneous systems like polymers and porous materials is referred to as anomalous diffusion and been reviewed by Metzler and Klafter.[17] ILs cannot be assumed to have such structures resulting in motional restrictions. Experimentally, the Δ-dependence D's for ILs have been observed in the lower temperature region especially in viscous ILs. As an example, the Δ-dependence observed for DEME-TFSA at 273 K are shown in Fig. 5. The diffusion plots following Eq. (1) are always linear with good precisions similar to an example shown in Fig. 2 for different protons of DEME in ^{1}H resonance and CF_3 in ^{19}F resonance.

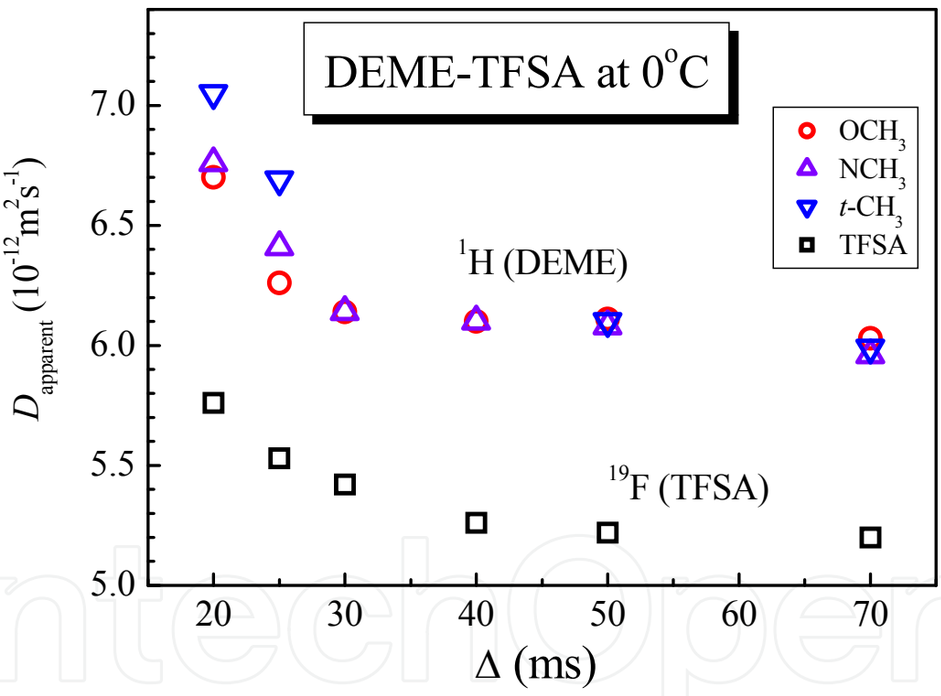

Fig. 5. The Δ-dependence of the apparent diffusion constant ($D_{apparent}$) for DEME (^{1}H) and TFSA (^{19}F) measured at 0 °C.

Clearly when Δ became shorter, apparent diffusion constant ($D_{apparent}$) became larger both in DEME and TFSA. At shorter Δ, the individual protons in DEME showed slightly different values. At the longer Δ, the $D_{apparent}$ values approached to equilibrated values for all proton signals and agreed within experimental errors. The similar experimental results were observed for ILs with high viscosity. Actually, DEME-TFSA does not show a Δ-dependence above 30 °C, while very viscous DEME-BF_4 showed significant Δ-dependent $D_{apparent}$ values at 30 °C. For the longer Δ values, each signal has the same values of $D_{apparent}$ and we adopt

such value as a diffusion coefficient D. In our experiments, we always observe values of $D_{apparent}$ for several Δ values and determine D at each temperature. Generally, in high temperatures the values measured in short Δ are adopted, while the values at long Δ are adopted in low temperatures.

5. Results

5.1 Temperature dependent T_1

Arrhenius plots of ^{1}H T_1 for various protons of the four cations are shown in Fig. 6 for EMIm, DMPIm, P_{13} and DEME. Since not all the protons show a T_1 minimum in their plots, the curves having minima are shown in solid marks. As a general trend, the protons located near the center of the molecules have T_1 minimum. For example, *t*-CH_3 of the propyl group in P_{13} gave the longest T_1 and did not exhibit a T_1 minimum, indicating that rapid local motion around the CH_3 group is contributed to T_1. Similarly, *t*-CH_3 in the ethyl group of EMIm did not give the T_1 minimum, while the *t*-CH_3 in the propyl group in DMPIm showed the T_1 minimum. When the T_1 minimum is observed, it is possible to calculate τ_c using Eq. (2).

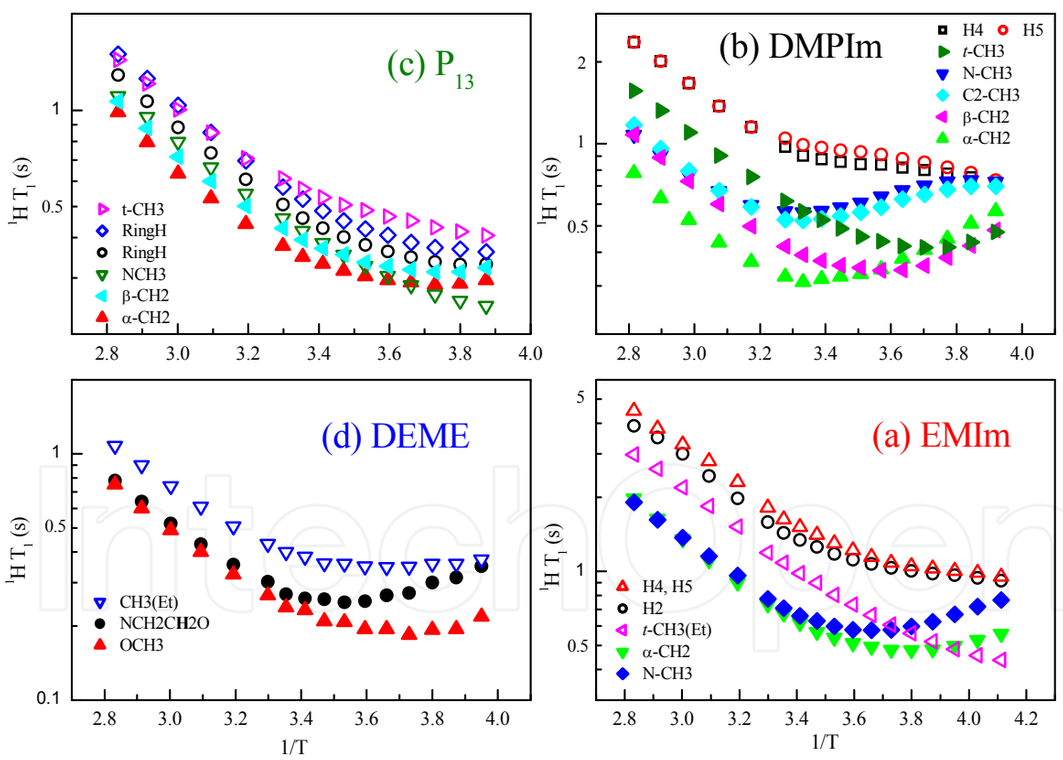

Fig. 6. Arrhenius plots of ^{1}H T_1 for the four cations, (a) EMIm, (b) DMPIm, (c) P_{13} and (d) DEME.

From Eq. (2), at the temperature of T_1 minimum, $\omega_0\tau_c = 2\pi\nu_0\tau_c = 0.616$ holds as described above. Since the present ν_0(H) = 270.17 MHz, $\tau_c = 3.63 \times 10^{-10}$ s (363 ps) at the T_1 minimum temperatures. From Fig. 6, it is possible to calculate τ_c values for each proton within a

molecule at every temperature. The dominant relaxation process showing ^{1}H T_1 minimum in the present temperature range can be assumed to be an isotropic motion of a whole molecule.

The calculated τ_c can be contributed by additional relaxation processes like fast local motions such as internal rotation around a three symmetrical axis in CH_3, segmental motions of alkyl chains, conformational exchange of imidazorium ring or ring inversional motion of pyrrolidinium ring as given in Eq. (4).

$$\frac{1}{\tau_c} = \frac{1}{\tau_o} + \frac{1}{\tau_s}, \tag{4}$$

where τ_o and τ_s are the correlation times for the isotropic reorientational and local intramolecular motions, respectively. Each proton having T_1 minimum afforded a little different τ_c values within a molecule. We adopted the longest τ_c values as the isotropic reorientational motion of a whole molecule, since the shorter τ_c values include the contribution of faster local motion. The Arrhenius plots of τ_c(cation) are shown in Fig. 7, and the activation energies are given in Table 2, where the τ_c(cation) values at 30°C are included. Since the Arrhenius plots are almost linear for the four ILs, the same mode of molecular motion is predominant to the T_1 process and the relaxation process is the isotropic reorientational motion. Clearly, the molecular rotation of DMPIm was the slowest in the whole temperature, and the other three cations have similar τ_c(cation) values at the high temperatures and in the low temperature range the isotropic motions are quicker in the order of P_{13}, EMIm, DEME and DMPIm.

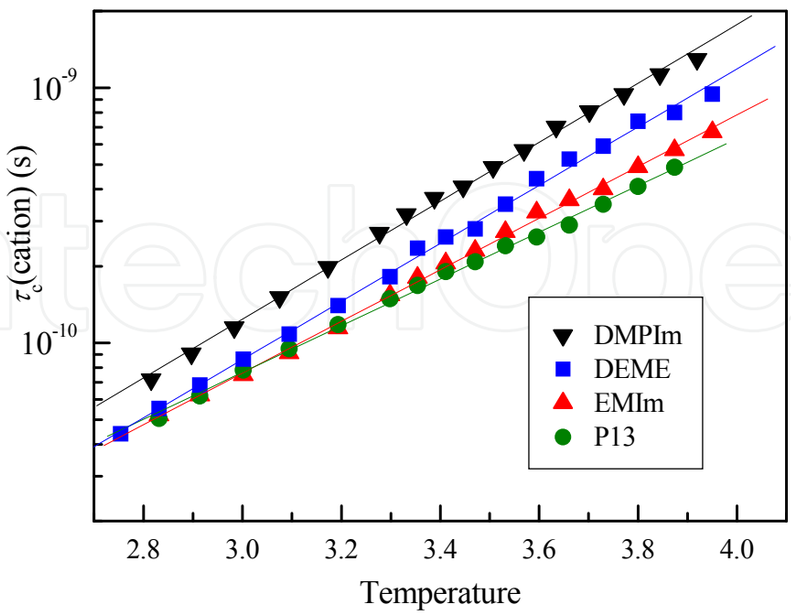

Fig. 7. Arrhenius plots of τ_c(cation) for the four ILs.

Cation	E_a for τ_c (kJ/mol)	τ_c at 30°C (s)	E_a for ^{19}F T_1 (kJ/mol)	
EMIm	19.4 ± 0.2	1.5×10^{-10} (15 ps)	14.4 ± 0.2 (above 40°C)	8.8 ± 0.2 (below 5°C)
DMPIm	22.1 ± 0.3	2.7×10^{-10} (27 ps)	15.4 ± 0.3 (above 40°C)	8.3 ± 0.2 (below 20°C)
P_{13}	17.5 ± 0.2	1.5×10^{-10} (15 ps)	14.1 ± 0.2 (above 30°C)	8.1 ± 0.2 (below 25°C)
DEME	21.8 ± 0.2	1.8×10^{-10} (18 ps)	10.2 ± 0.2 (above 40°C)	7.1 ± 0.4 (below 20°C)

Table 2. The activation energies E_a (kJ/mol) of the τ_c for the cation motion and the τ_c (s) at 30°C, and the E_a (kJ/mol) for ^{19}F T_1 of CF_3.

As shown in Fig. 6, the protons of the imidazolium rings of EMIm and DMPIm showed longer T_1 than those of the side chains and in the low temperature region the T_1 values did not increase. In other words T_1 minimum was not observed for the imidazolium ring protons. In the present discussion, the reorientational motion should affect significantly ^1H T_1 of the ring protons.

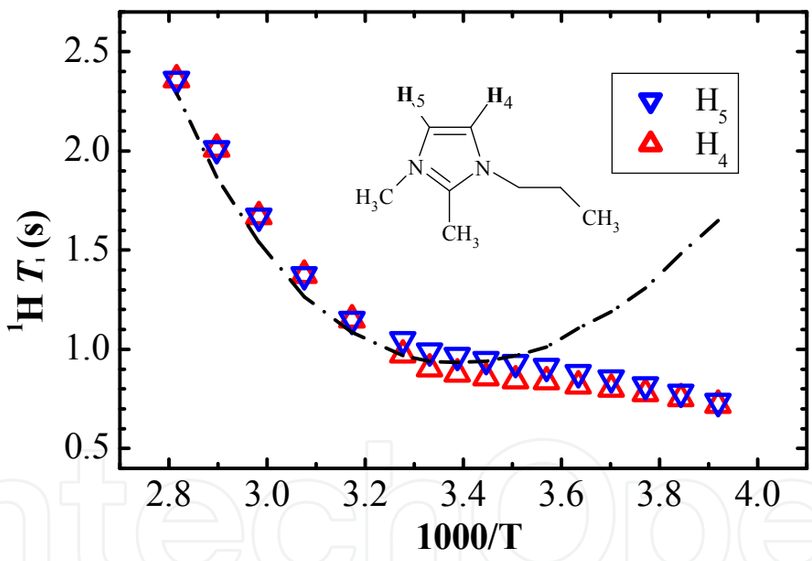

Fig. 8. The observed T_1 values of H_4 and H_5 of the imidazolium ring of DMPIm and the calculated T_1 (dotted line) for the H_5 using the τ_c(DMPIm) in Fig. 6 and Eqs. (2) and (3).

The trial was made to calculate the T_1 values for the H_5 of DMPIm using the τ_c(DMPIm) in Fig. 7. Here the H-H distances for the H_5 between H_4 and CH_3 were included. Clearly, above 303 K the calculated T_1 of H_5 agreed with the observed T_1's of the H_4 and H_5 of which the T_1 values were almost the same. As the temperature decreased, the observed T_1 became shorter since additional fast relaxation mechanisms become operative. The calculations were made for the ^1H T_1 for the H_4 and H_5 of the imidazolium protons in EMIm and the similar results were obtained.[4] In the low temperature, the rate of the isotropic reorientation of the whole molecule becomes slower and the long T_1 is reduced by local motions such as planar-

nonplanar conformational changes of the imidazolium ring changes having the activation energy of about 5 kJ/mol observed by Raman spectroscopy.[18]
Arrhenius plots of ^{19}F T_1 of CF_3 in TFSA are shown in Fig. 9 for the four ILs. The plots are curved and the activation energies were calculated for the higher and lower temperature regions as given in Table 2. Two relaxation processes are possible for the ^{19}F T_1, i. e. the internal rotation around the three-symmetrical axis and the isotropic reorientational molecular motion. Probably an overall molecular motion is the major relaxation process in the high temperature region with larger activation energies and the internal rotation of the CF_3 contribute predominantly to the ^{19}F T_1 in the lower temperature region with the smaller activation energies. Among the four ILs, the values of ^{19}F T_1 of the TFSA in EMIm-TFSA are much longer than those of the other three ILs, owing to faster motions of the fluorine atoms in the smallest viscosity.

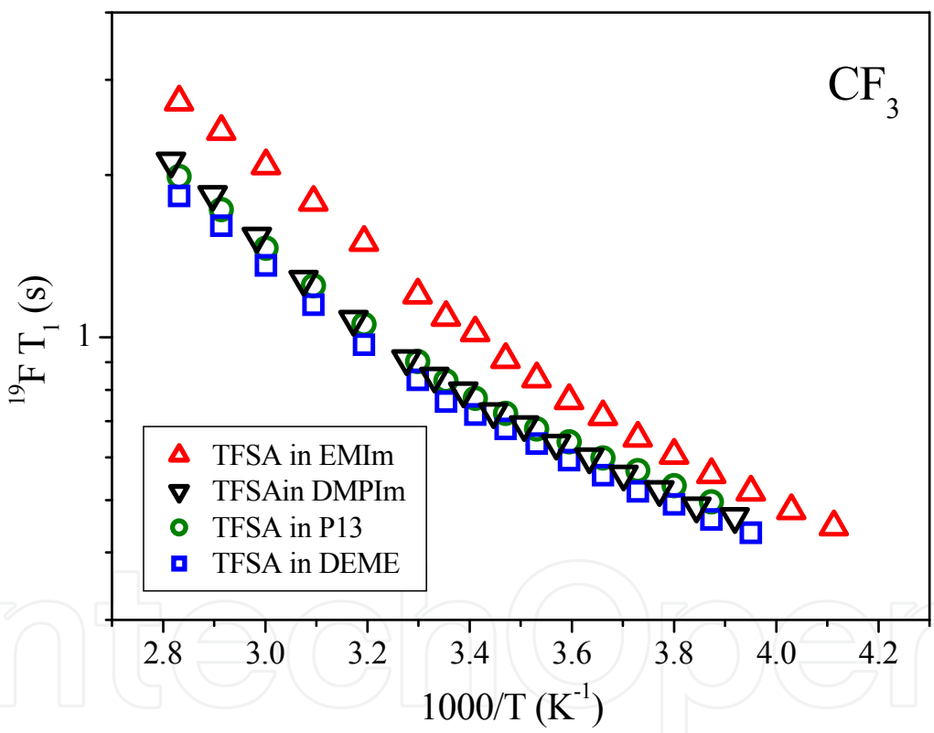

Fig. 9. Arrhenius plots of ^{19}F T_1 for CF_3 of the TFSA in the four ILs.

5.2 Translational diffusion

The diffusion coefficients are plotted versus temperature in Fig. 10 for (a) cations and (b) TFSA. The order of D_{cation} and D_{TFSA} is EMIm > P_{13} > DEME > DMPIm, which is consistent with the order of $1/\eta$ in Table 1. Within the same IL it always holds $D_{cation} > D_{TFSA}$ in the present four ILs.

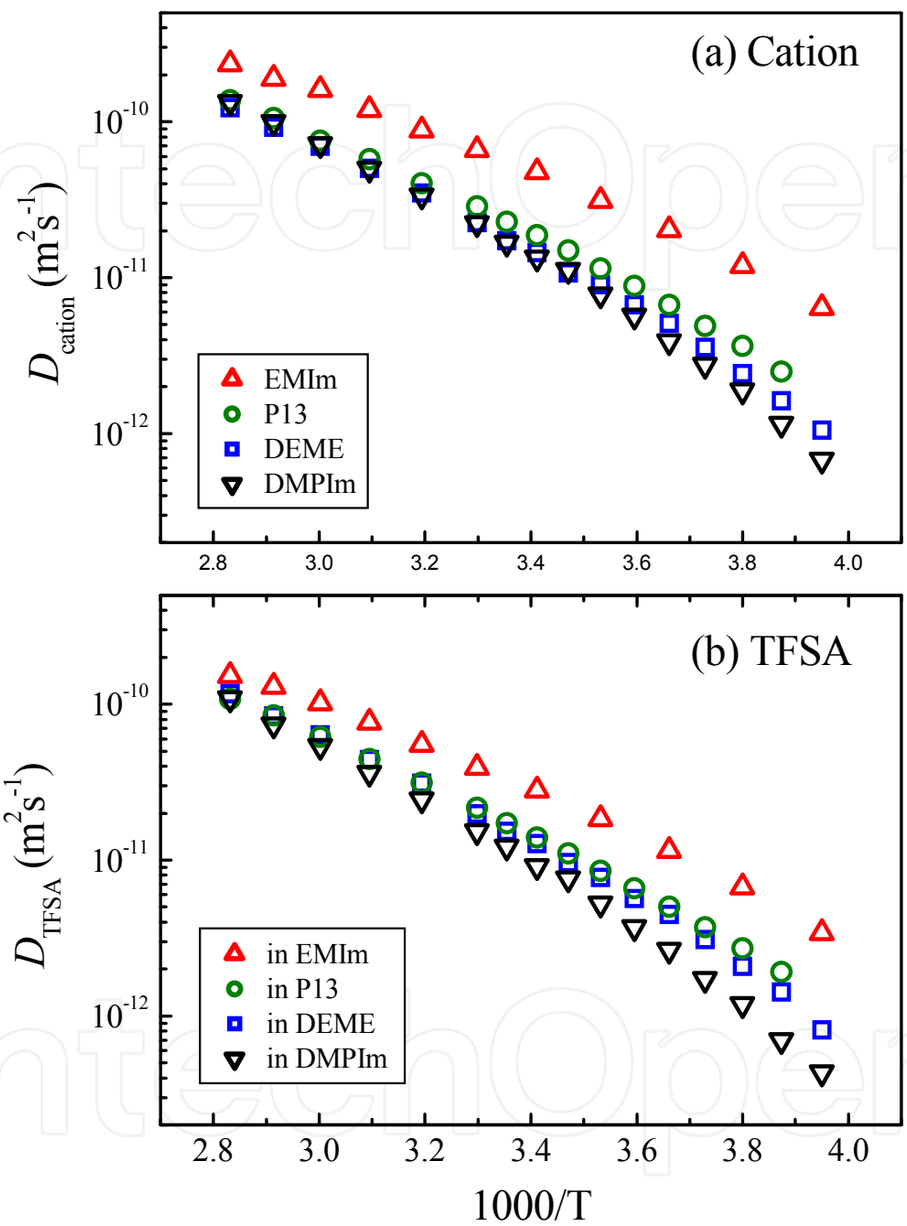

Fig. 10. (a) The D_{cation} and (b) the D_{TFSA} are plotted versus temperature.

5.3 Viscosity, ionic conductivity and density

The viscosity (η) is plotted versus temperature in Fig. 11(a) and the Arrhenius-type plots were made for 1/η for inverse of temperature in Fig. 11(b) for the four ILs.

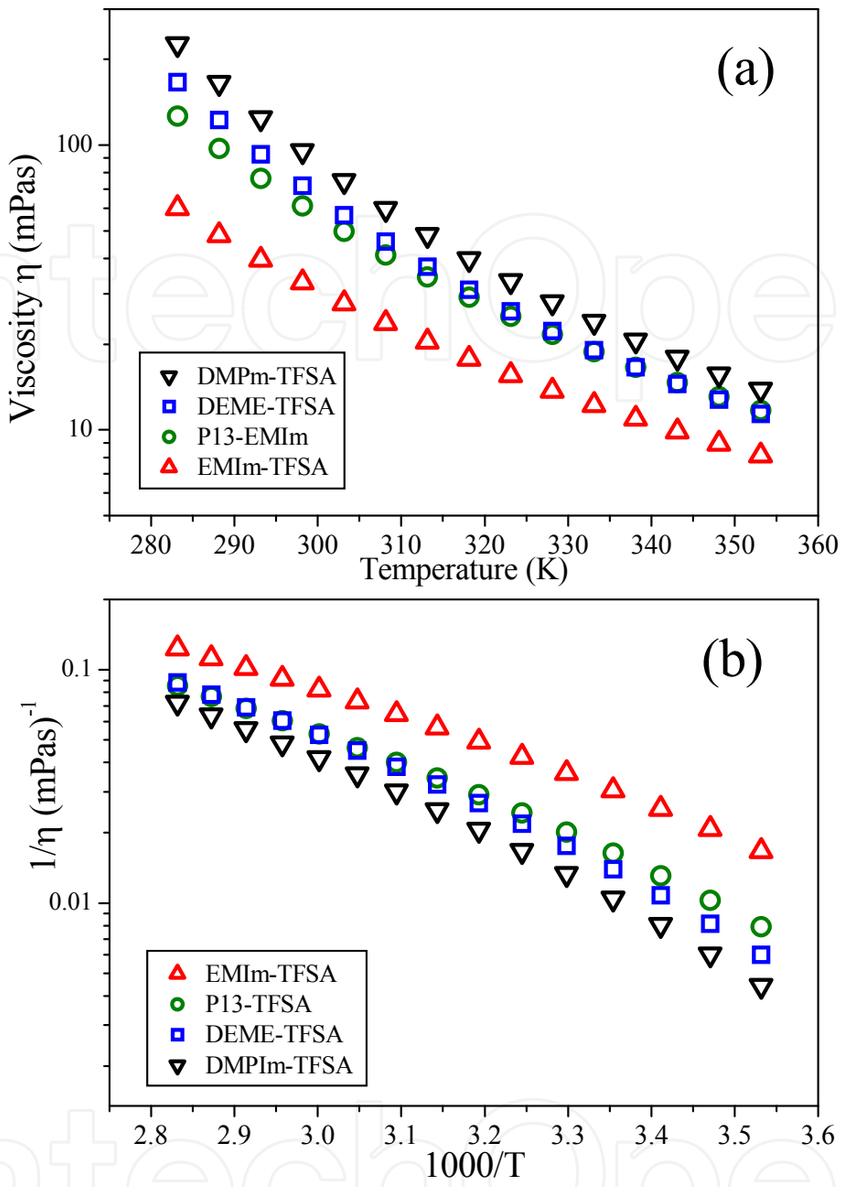

Fig. 11. Temperature dependent viscosity for the four ILs (a) η vs temperature and (b) Arrhenius plots of 1/η.

The viscosity differences among the ILs became small at the higher temperature. In the low temperature region the order of the viscosity is EMIm-TFSA << P_{13}-TFSA < DEME-TFSA <DMPIm-TFSA. The values of η at 30°C are given in Table 1.

The ionic conductivities (σ) of the four ILs are plotted in Fig. 12 and the order of the magnitudes is EMIm-TFSA >> P_{13}-TFSA ≥ DEME-TFSA ~DMPIm-TFSA. The largest σ for EMIm-TFSA was obtained for the smallest η.

The densities are plotted against temperature in Fig. 13. The order is EMIm-TFSA >> DMPIm-TFSA > P_{13}-TFSA > DEME-TFSA and for reference the order of the molecular weight given in Table 1 is EMIm-TFSA < P_{13}-TFSA < DMPIm-TFSA < DEME-TFSA.

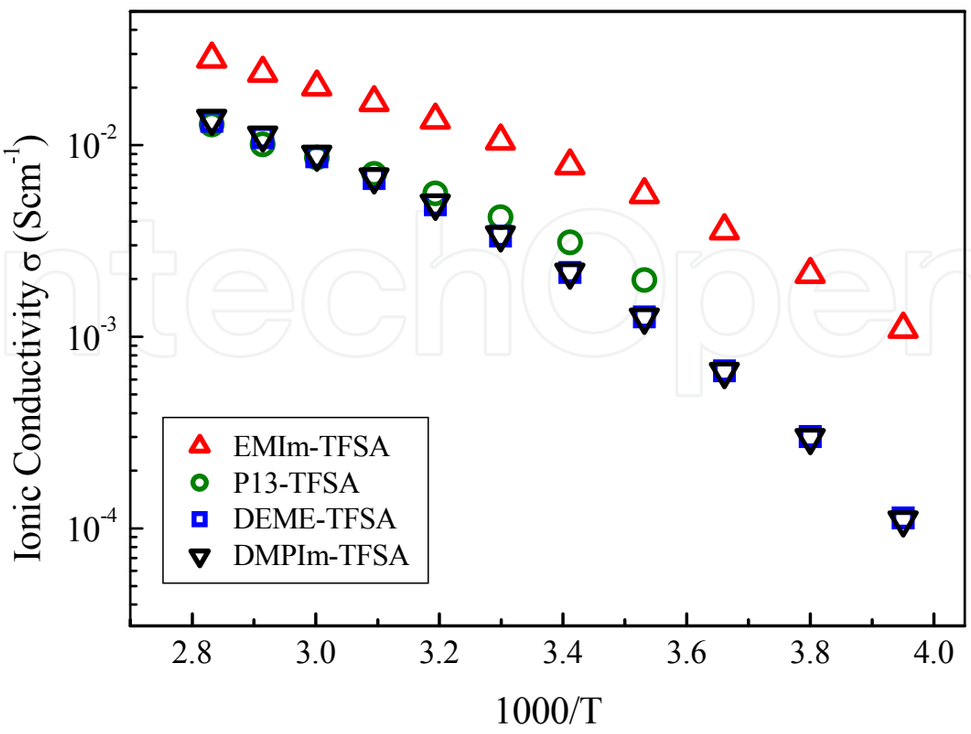

Fig. 12. The temperature dependence of ionic conductivity for the four ILs

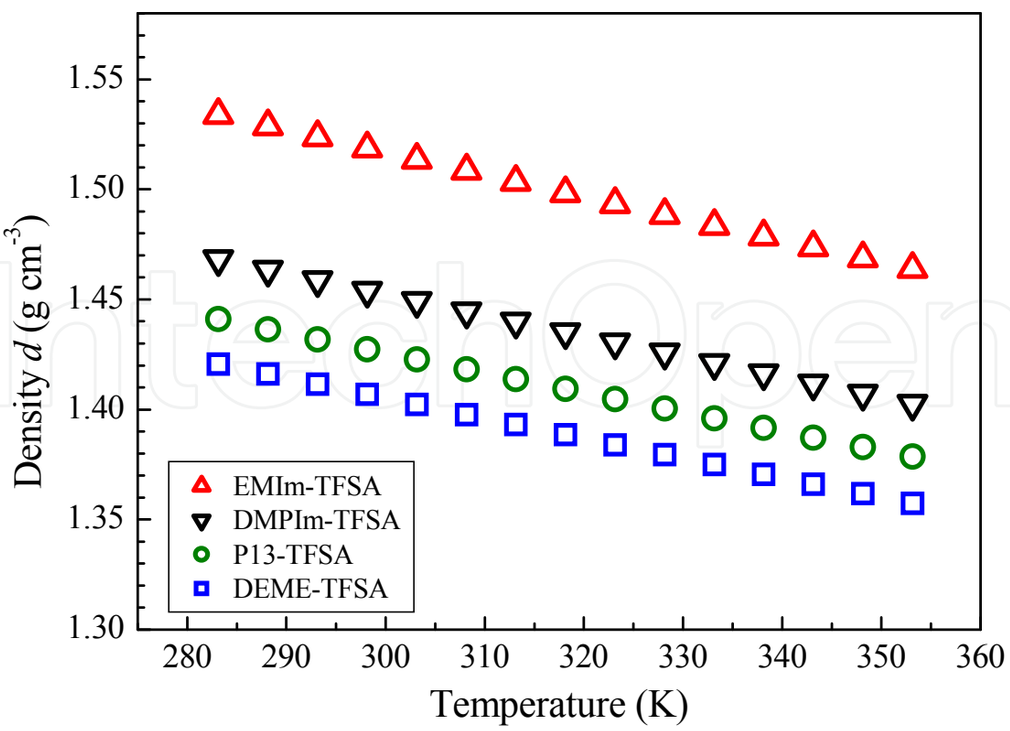

Fig. 13. The densities are plotted against temperature for the four ILs.

6. Discussion

6.1 Stokes-Einstein relation

By the classical Stokes-Einstein (SE) (or Einstein-Sutherland) relation we will describe our experimental results between the individual ion diffusion coefficients in Fig. 10 and the viscosity in Fig. 11. The SE equation is given as

$$D = \frac{kT}{c\pi\eta a} \tag{4}$$

where a is the radius of the diffusing species, k is the Boltzmann constant and the constant c theoretically ranges between 4 to 6 for slip and stick boundary conditions, respectively.[16,19] In the limit of the slip condition (c = 4), no interaction is assumed between a particle and surrounding molecules. When a particle interacts strongly with solvent molecules, the stick condition holds (c = 6). Here, we attempted to plot the experimentally determined D versus $1/\eta$ according to the classical SE by assuming that c is an empirical parameter. The D values are plotted against $kT/\pi\eta$ for (a) D_{TFSA} and (b) D_{cation} of the four samples in Fig 14. When we presume that the SE equation is valid, the gradient of each line corresponds to the inverse of $c \times a$. In Fig. 14 the plots are linear for the all ions. The experimental values of $c \times a$ are summarized in Table 3, where the errors estimated for the linear plots were less than 3 %. Clearly, the classical SE relationship (4), i.e., $D \propto 1/\eta$ can be used to obtain physical meaning between the translational ion motion and bulk viscosity in the present four ILs. Here we assume that the van der Waals radius calculated from the van der Waals volume can be used as the radius of diffusing ion as given in Table 3.

Ion	Counter ion	c × a (nm)	Van der Waals volume (nm^3)	Van der Waals radius (nm)	c
EMIm	TFSA	0.833 ± 0.016	0.11756	0.304	2.7_5
DMPIm		0.850 ± 0.061	0.15053	0.330	2.5_6
P_{13}		0.982 ± 0.013	0.15025	0.330	2.9_8
DEME		1.138 ± 0.007	0.17806	0.349	3.2_6
TFSA	EMIm	1.323 ± 0.019	0.14950	0.329	3.7_5
	DMPIm	1.162 ± 0.013[a)]			3.5_3
	P_{13}	1.228 ± 0.013			3.7_3
	DEME	1.204 ± 0.018			3.6_6

[a)]Two points in DMPIm were not included for the calculation, which were largely deviated in the low temperature region

Table 3. SE relationships for each ion in the four ILs.

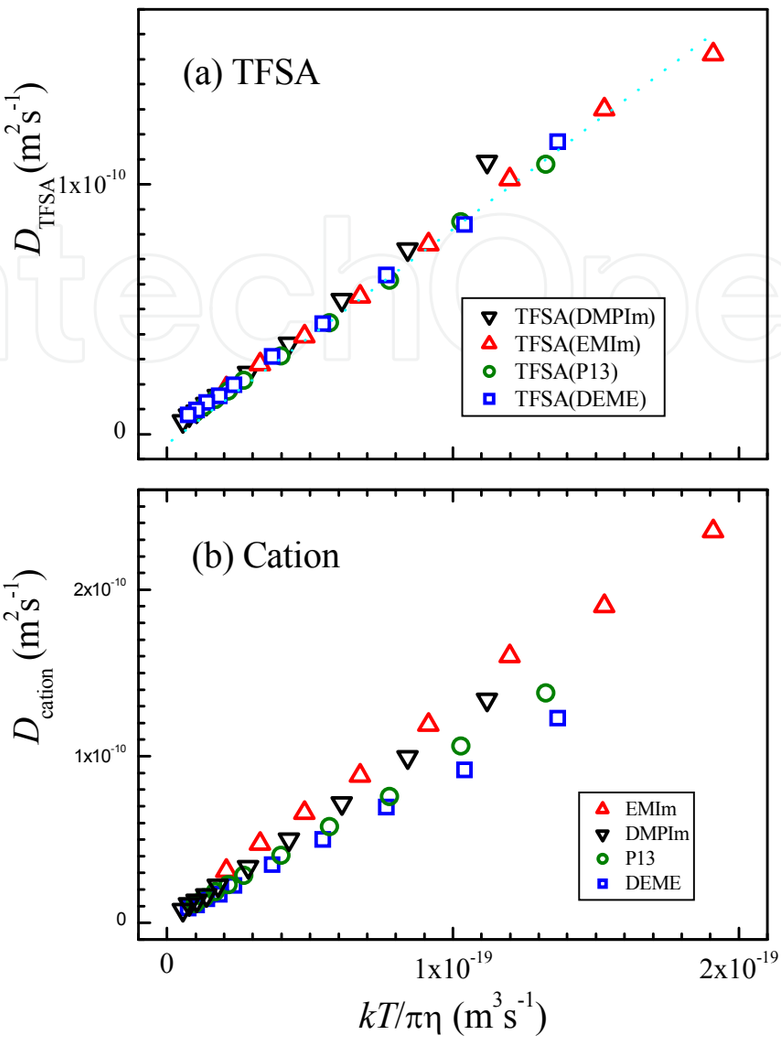

Fig. 14. Diffusion coefficients were plotted *vs* $kT/\pi\eta$ for (a) TFSA and (b) cations.

It is noted that the *c* values of TFSA range between 3.5 and 3.8 and the cations have the smaller *c* values compared to TFSA. Previously we have reported that the *c* values of bis(fluorosulfonyl)amide (FSO_2-N$^-$-SO_2F, FSA, MW = 180.1 and van der Waals radius = 0.284 nm) are 2.8 and 3.1 for EMIm-FSA and P_{13}-FSA, respectively. Also, the *c* values of EMIm and P_{13} were 2.5 and 3.0 in the FSA-based ILs.[3,4] The *c* values are purely empirically derived parameters for individual ions in neat ILs based on the SE equation. As a general trend, ions in ILs have their individual *c* values. The empirical c values are smaller than 4, the theoretically predicted smallest limit. Experimental values were calculated as $c \times a$ for each ion. If we assume the size of the diffusing ions become larger owing to the ion association, the *c* values becomes smaller. The classical SE relation was derived for a diffusing rigid particle with radius *a* in a medium having viscosity η. Ionic liquids are quite different materials from the assumptions of the SE equation. Fractional SE relation (F-SE) has been proposed to explain the relation between *D* and *η* as $D \propto (T/\eta)^m$.[20-22] We attempted to apply the F-SE and found that even when the extra parameter *m* was introduced, the fitting in the linear plots ln(*D*) versus ln($kT/\pi\eta$) were not much improved.

6.2 Walden plot

Walden's rule in electrochemistry describes the relationship between ionic conductivity σ with viscosity η, that is, σ × η = constant.[23] The electrochemical molar conductivity (Λ_{imp}) can be calculated from ionic conductivity as $\Lambda_{imp} = \sigma M/\rho$, where M is the molecular weight and ρ is the density. The Walden plots of the molecular conductivity versus $1/\eta$ in the unit of 0.1 Pas (=poise) proposed by Angell and coworkers[24] are shown in Fig. 15 for the present four ILs. The Walden rule relates the molecular mobility ($1/\eta$) to the molar conductivity induced from the charged ions in solution electrolytes and characterizes ILs. The fully dissociated ions such as diluted aqueous KCl solution give a behavior shown as a line in Fig. 15. The deviation from the ideal plot, ΔW has been proposed to relate with the ion pairing of ILs.[25] In the present ILs, the ΔW for EMIm-TFSA exhibited the smallest value, followed by DMPIm-TFSA, DEME-TFSA and P_{13}-TFSA.

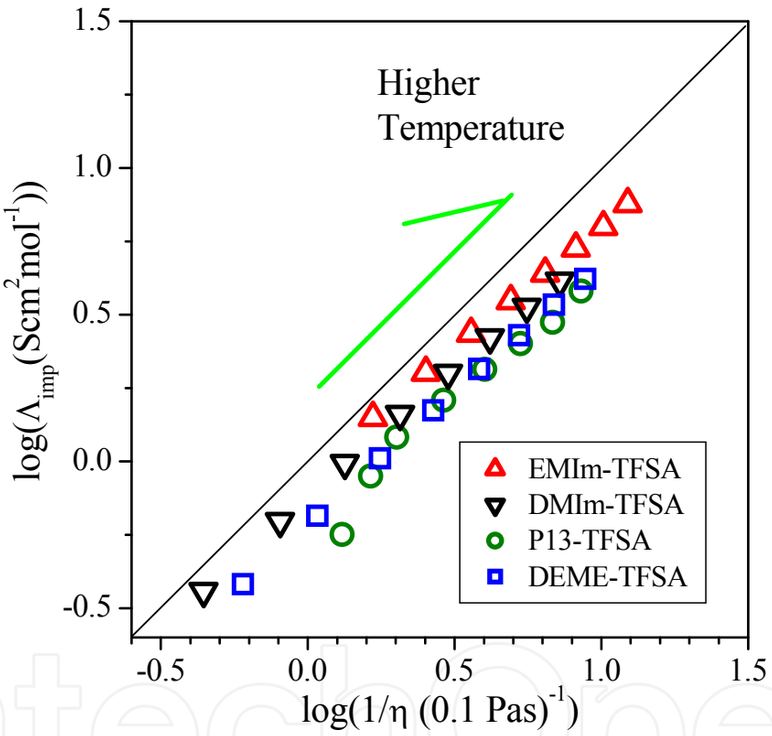

Fig. 15. Walden plots for the four ILs.

6.3 Nernst-Einstein relation

The relationship between the ion diffusion and ionic conductivity has been studied by the Nernst-Einstein (NE) equation (5) for molar conductivity Λ.

$$\Lambda = \frac{zF^2}{RT}(D_+ + D_-), \tag{5}$$

where z is the ionic valency, F is Faraday's constant, R is gas constant, and D_+ and D_- are the self-diffusion coefficients of the cation and anion, respectively under the assumption of complete ion dissociation.[23] Studies of aqueous electrolytes have been made to verify the NE

equation. It is known that when a salt concentration increases, the modification of the original NE equation is necessary to give Eq. (6)

$$\Lambda_{NE} = \frac{zF^2}{RT}(D_+ + D_-)(1-\xi), \tag{6}$$

where ξ is a parameter to relate with the ion association. Then 1-ξ means a degree of ion dissociation. In the early stage of our studies for PGSE NMR diffusion measurements of solution electrolytes, we verified that Eq. (6) is valid for electrolytes including lithium salts in organic solvents (propylene carbonate and γ-butyrolactone) near the infinitesimal concentration by measuring the ion diffusion coefficients and ionic conductivity. As the concentration of the salt increased, the values of 1-ξ became smaller to indicate the promotion of ion association. The diffusion coefficients of the solvents became smaller as the increase of the salt concentration owing to the increase of viscosity.[26] Since the PGSE self-diffusion measurements reflect the average *D*'s for species in both free and associated forms, the value of the NMR molar conductivity (Λ_{NMR}) calculated using Eq. (5) ($\Lambda = \Lambda_{NMR}$) is always overestimated. The calculated Λ_{NMR} and Λ_{imp} are plotted versus temperature in Fig. 16 for the four ILs. Clearly the Λ_{NMR} values are always larger than Λ_{imp}, and precise watching indicates that the relationship between the Λ_{NMR} and Λ_{imp} are a little different dependent on temperature and ILs.

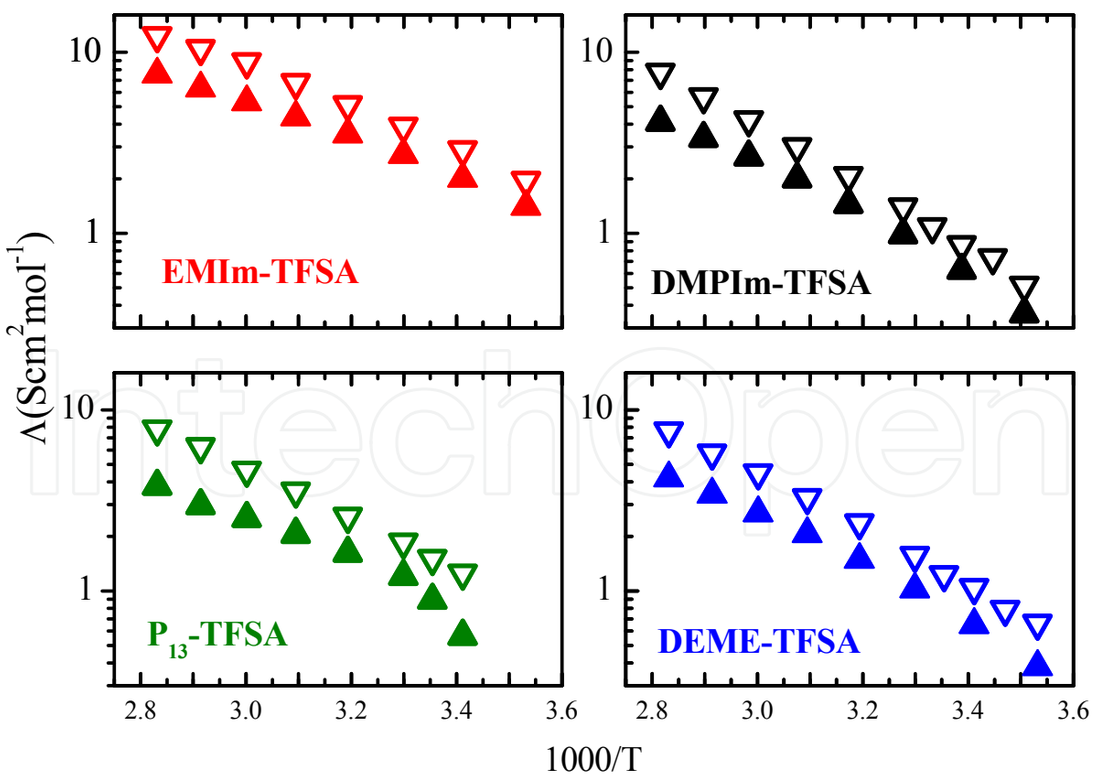

Fig. 16. The molar conductivities derived from ionic conductivity Λ_{imp}(solid) and NMR Λ_{NMR}(open) are plotted versus temperature for the four ILs.

The Λ_{imp} can be obtained from the electrochemical impedance method by measuring only the charged ions. The relationship between ionic conductivity σ and the mobility μ of ions is expressed as $\sigma = nq\mu$, where n is the number of carrier ions, q is the electric charge of ions and μ is the mobility of ions. The ion mobility can be assumed to be parallel to the D, although the question remains whether isolated and paired ions diffuse with the same diffusion coefficients. The actual values are averaged ones. The discrepancy between Λ_{imp} and Λ_{NMR} is considered to be related to the relative numbers of the charged and paired ions, and/or the lifetime of the paired ions. Then, the Haven ratio, $\Lambda_{imp}/\Lambda_{NMR}$, calculated as the ratio of Λ_{imp} divided by the Λ_{NMR} has been named as "ionicity" of ILs proposed by Tokuda et al[27-28] and is related to the ratio of the charge carrying ions. Previously, no temperature dependence of the ionicity was observed, but our recent measurements indicate a decrease in ionicity with increasing temperature.[1-4] The $\Lambda_{imp}/\Lambda_{NMR}$ values of the four ILs are plotted against temperature in Fig. 17 and it is shown that the temperature dependent behaviors of the $\Lambda_{imp}/\Lambda_{NMR}$ are a little different with each other for the individual ILs.

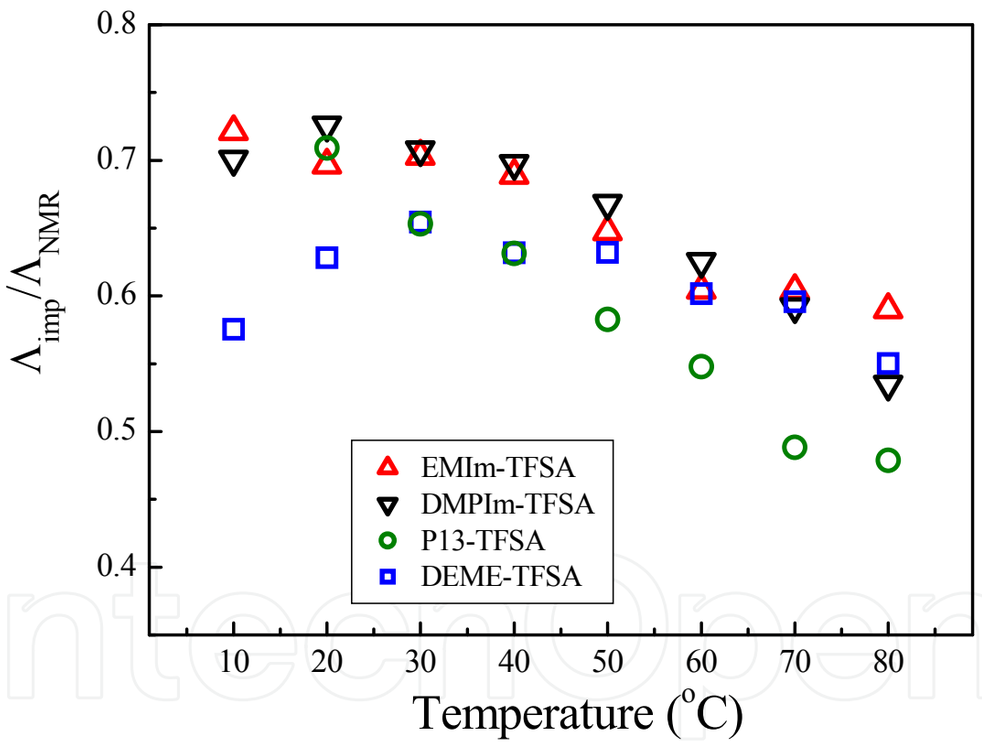

Fig. 17. The $\Lambda_{imp}/\Lambda_{NMR}$ (ionicity) are plotted *vs* temperature for the four ILs.

The experimental values of $\Lambda_{imp}/\Lambda_{NMR}$ were calculated from the empirical values of σ, ρ, D_{cation}, and D_{anion}, all of which were measured independently. Even if an error bar of each measurement is small, the scattering of the $\Lambda_{imp}/\Lambda_{NMR}$ can easily become larger. In the higher temperature region, the values of EMIm-TFSA, DMPIm-TFSA and DEME-TFSA are similar and that of the P_{13}-TFSA is smaller than the other three ILs. When the temperature decreased, the value of DEME-TFSA decreased largely. Generally, the $\Lambda_{imp}/\Lambda_{NMR}$ values became smaller as the higher temperature region.

From Eqs. (5) and (6), $\Lambda_{imp}/\Lambda_{NMR}$ corresponds to 1-ξ, which is defined as the degree of ion dissociation or ion dissociation parameter in aqueous and organic solution electrolytes. It has been established that (1) as the ion concentration increases, the η increases and the σ decreases owing to the formation of ion pairs, and (2) when the η increases, the *D* decreases without distinguishing isolated or paired ions. The degree of ion dissociation 1-ξ (=1 is the complete ion dissociation) has parallel relationships with 1/η, σ and *D* and increases with the increase of temperature for series of a solution electrolyte. The empirical behaviours of $\Lambda_{imp}/\Lambda_{NMR}$ for the ILs in Fig. 17 conflict with general concepts that ion dissociation becomes larger in higher temperature. Comparing the Arrhenius plots of ionic conductivity (Fig. 12), $1/\eta$ (Fig. 11 (b)) and diffusion coefficients (Fig.10), the curvatures in the ionic conductivities were larger than those of the other parameters in the high temperature region. Phenomenologically, the decreasing trends of $\Lambda_{imp}/\Lambda_{NMR}$ in the higher temperature region can be interpreted from the facts that Arrhenius plots of the ionic conductivity for most ILs are curved significantly at the high temperatures and the values do not increase as expected from viscosity and ion diffusion coefficients.

We must say that "ionicity" in ILs is not a static "degree of ion dissociation" as pointed out by Harris,[29] but the original definition of "ionicity" as the ratio of the charge carrying ions by Watanabe's group may be still valid. The experimental facts that the $\Lambda_{imp}/\Lambda_{NMR}$ increases with the increase of the viscosity is very strange and conflicts with the general properties of solution electrolytes. More precise studies are necessary to connect experimental "ionicity" ($\Lambda_{imp}/\Lambda_{NMR}$) to ion pairings in ILs including timescales of ionic interactions, such as dynamic ion associations and static ion-ion interactions.

6.4 Cation molecular motion

We assume that the ^{1}H correlation time τ_c for the cations in Fig. 7 corresponds to whole molecular motion rather than intramolecular local motions. The segmental motion of alkyl substituents and CH_3 rotational motion are accelerated and averaged out in the condensed state. The activation energies for the τ_c(cation) in Table 2 are 17 to 22 kJ/mol in the temperature range studied. The conformational change of the ethyl chain attached to imidazolium ring for EMIm has been reported to take place with activation energies about 5 kJ/mol.[18] Similarly, the activation energies of the pseudo-rotation of the pyrrolidinium ring was reported to less than 5 kJ/mol.[30-31] Then, the motion of a whole molecule can contribute to the temperature-depending ^{1}H T_1 having T_1 minima. The activation energies for translational diffusions (26, 30, 32 and 33 kJ/mol for EMIm, P13, DEME and DMIm, respectively for the linear plots in the higher temperature regions in Fig. 10 (a)) are much larger. In NMR relaxation theory, the translational correlation time can be defined as $\tau_c = 2a^2/D$ following Abragam,[32] where a is the radius of the diffusing particle. The temperature dependences of τ_t values for the four cations are shown in Fig. 18 together with the τ_c(cation) values obtained from the ^{1}H T_1.

The overall isotropic molecular correlation time τ_2 is related to the viscosity η by the Stokes-Einstein-Debye (SED) relation as

$$\tau_2 = \frac{V\eta}{kT} \tag{7}$$

where V is the effective molecular volume. The model was originally proposed for rotational time of a solute in a solvent of the shear viscosity η. Significant studies have been reported about the SE and SED relationships based on MD simulations, and the validities and limitations of the SE and SED have been discussed.[33,34] Experimental studies on the rotational motion of small molecules dissolved in ILs have also been reported.[35-39] We calculated τ_2 in Eq. 7 by using the measured viscosity data and assuming V of the van der Waals volumes of the cations in Table 3. The calculated τ_2 values are also shown in Fig. 18 together with the τ_c and τ_t values for the temperature range between 283 and 353 K.

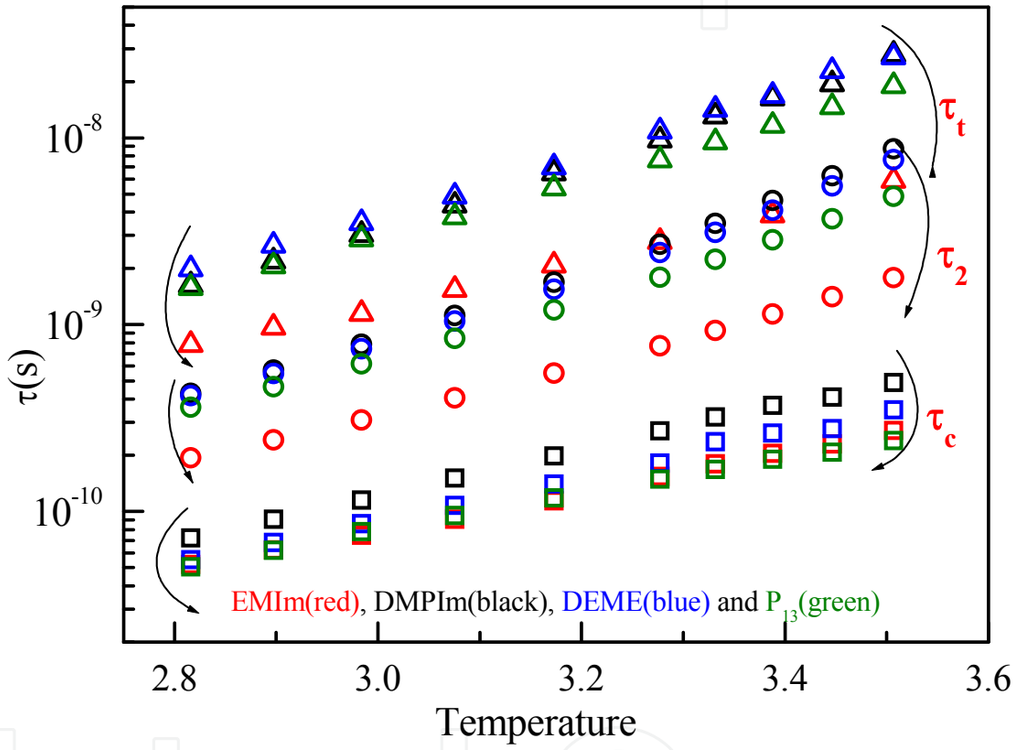

Fig. 18. Temperature dependences of the correlation times τ_c for librational motion, τ_2 for reorientational motion and τ_t for translational motion of the four cations.

The τ_c values evaluated from NMR relaxation times are always shorter than the values estimated using the SED model. The NMR relaxation takes place for one motion of a single dipole-dipole flip and can describe the time interval for the motion but not the amplitude. As proposed in our previous papers,[1-4] we assume that the τ_c process is the small-angle librational motion of the cation. Assuming the τ_2 value calculated from η correspond to a 360° rotation, the angles for the librational motions were calculated and plotted versus temperature in Fig. 19. The flip angle for EMIm is particularly larger than those for the other anions. The molecular flip amplitude becomes smaller at lower temperature.

In the present study, we propose experimental correlation times for the three different modes of motion with different times, i.e. τ_t, τ_2 and τ_c derived from the experimental data of D_{cation}, η (and the volume) and ^{1}H T_1 of the cations, for the translational, molecular overall

rotational and librational motions of the cations, respectively. Clearly, the order was τ_c (librational) < τ_2 (overall molecular rotation) < τ_t(translation) for the all cations in the present temperature range. It is noted that although the values τ_c for EMIm enter the values of the other cations, the τ_t and τ_2 for EMIm are particularly short compared with those of the three cations probably due to the extremely small viscosity of EMIm-TFSA.

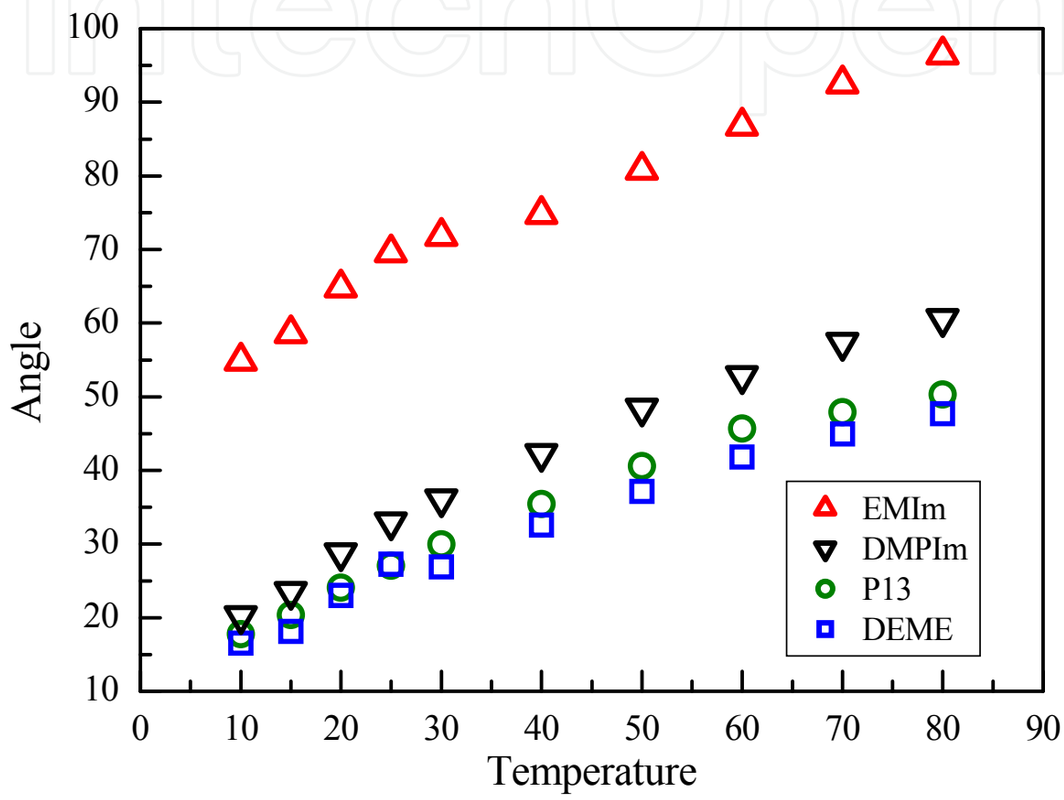

Fig. 19. The flip amplitude of the cations versus temperature for the four cations.

6.5 Relationships of τ_c(cation) with η and *D*

The τ_c(cation) is defined as a time of a motion for the librational flip of a whole molecule. An attempt was made to plot the τ_c(cation) versus viscosity as shown in Fig. 20. When the viscosity is small (about less than 50 mPas) above room temperature, the relations between the τ_c(cation) and the bulk η are linear, while in the lower temperatures, the plots were curved and the gradients became smaller. It is clearly shown that the viscosity became larger, the time interval for the librational flip of the cation became longer. The larger gradients for the relations τ_c(cation) versus η were obtained for EMIm and DMPIm having imidazolium rings and P_{13} exhibited the smallest gradient. The rate of the librational motion is proportional to the bulk viscosity.

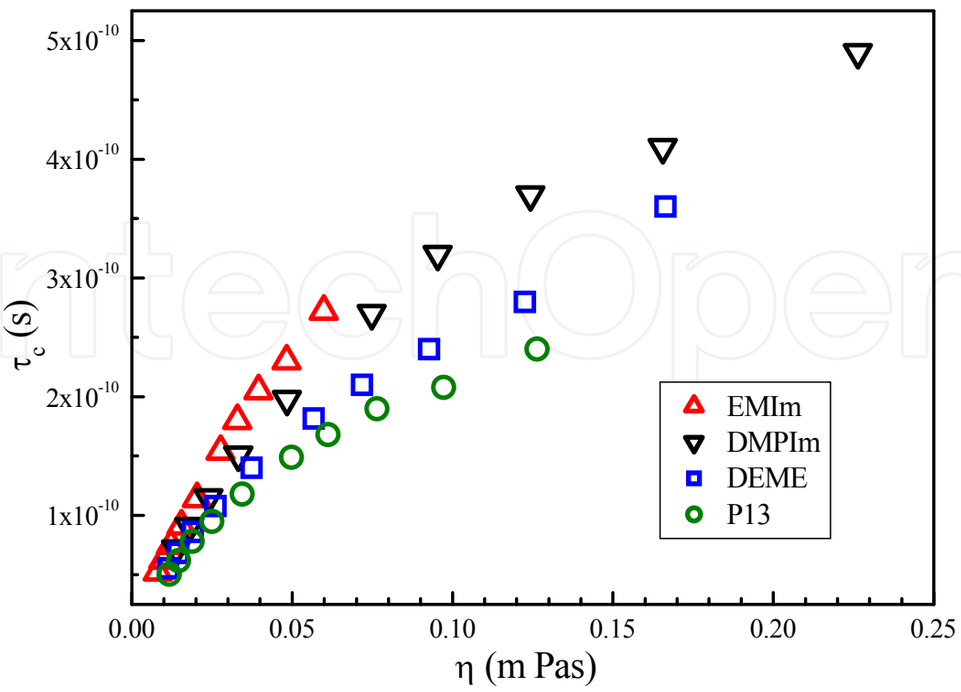

Fig. 20. The τ_c was plotted versus viscosity for the four cations.

Log-log plots of the D_{cation} versus the τ_c(cation) are shown for the four cations in Fig. 21. Although the plots are curved, the D_{cation} and the τ_c(cation) are clearly correlated.

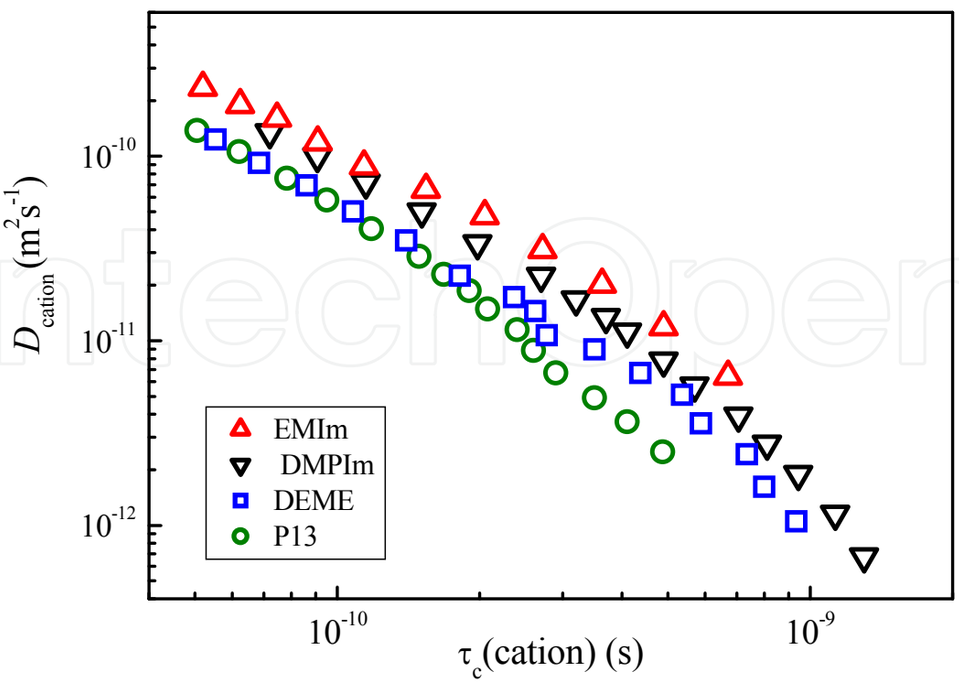

Fig. 21. The plots of D_{cation} versus τ_c(cation) for the four cations.

It is interesting to compare the Arrhenius plots of D_{cation} in Fig. 10 (a) and the plots of D_{cation} against τ_c(cation) in Fig. 21. Since the viscosity of EMIm-TFSA is much smaller compared with that of DMIm-TFSA, D_{EMIm} is much faster than D_{DMPIm} at the same temperature as shown in Fig. 10(a), while the D's are closer for the same τ_c(cation) in Fig 21, suggesting the correlation time of librational flip is related to translational diffusion.

Next, the values of the D_{cation} were plotted against the rates of librational motion ($1/\tau_c$(cation)) as shown in Fig. 22. Although the plots were bent, linear relations were obtained. EMIm exhibited the linear relation in the whole temperature range. The gradients were calculated for the plots D_{cation} versus $1/\tau_c$(cation) above and below 30°C. Since the unit of the gradients is m^2, the square root values are summarized in Table 4 as a diffusion distance during one-flip for each cation. Except for EMIm they became a little longer in the higher temperature region. It is noted that the distance is not sensitive to temperature. As a general trend, the distances are in the order for EMIm ~ DMPIm > P13 ~ DEME. Since the distance is much smaller than the van der Waals radius given in Table 3, translational movement is closely coupled with a molecular librational flip. In other words, the distance for translational movement of the cation during one flip is smaller than the molecular size. The librational flip and translational motion are strongly coupled, and the translation takes place by accompanying librational flip motions. The diffusion scheme for the cation in ILs is different from the rigid-body diffusion model which is the basic concept to drive the SE relation.

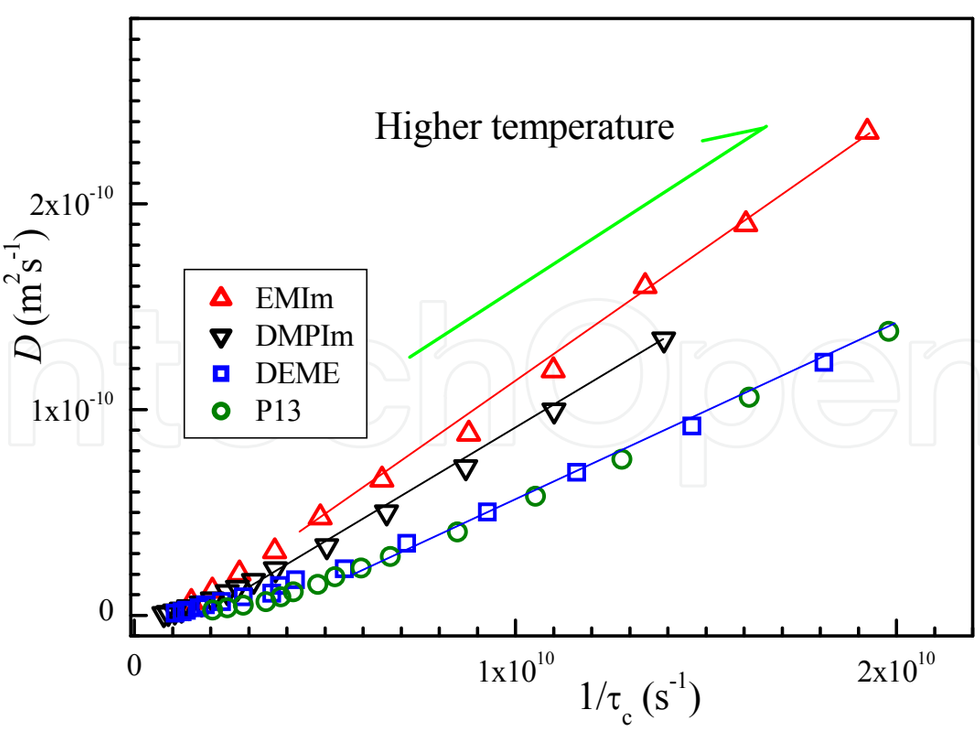

Fig. 22. The D_{cation} is plotted versus the rate of the librational flip.

	Above 30°C	Below 30°C
EMIm	$0.11_4 \pm 0.002$	
DMPIm	$0.12_2 \pm 0.002$	$0.08_3 \pm 0.02$
P13	0.09 ± 0.01	0.07 ± 0.02
DEME	0.09 ± 0.01	0.07 ± 0.02

Table 4. Translational distances during a librational flip of the cations (nm)

6.6 CF_3 motion of TFSA

The Arrhenius plots of ^{19}F T_1 for CF_3 of the TFSA in Fig. 8 were almost linear and the T_1(F) values became longer as the temperature increased, indicating the ^{19}F relaxation takes place under the extreme narrowing condition, i. e. $\omega_F \tau_c(F) << 1$ and thus, $\tau_c(F)$ is proportional to $1/T_1(^{19}F)$. In Fig. 23, the viscosity was plotted against $1/T_1(^{19}F)$. The tendency exists that the $\tau_c(F)$ is affected by the bulk viscosity and became longer as the viscosity increased.

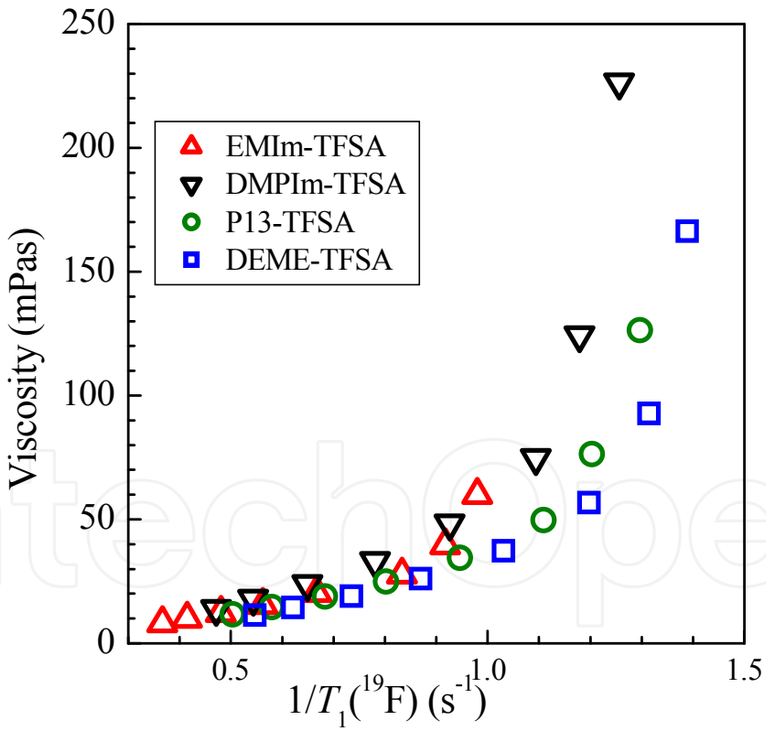

Fig. 23. The viscosity was plotted versus $1/T_1(^{19}F)$ of CF_3.

7. Conclusion

The motions of cations for the four TFSA-based ILs with EMIm, DMPIm, P_{13} and DEME were studied by ^1H NMR spectroscopy by measuring the self-diffusion coefficient (D) and

^{1}H spin-lattice relaxation time (T_1). The correlation time τ_c for the cation motion was derived from the Arrhenius plots of T_1 where the T_1 minimum was observed. The relationship of the D and τ_c suggests that the translational motion is coupled with a small-angle librational flip of the cation. In other words, the position change of a cation takes place by accompanied with a flip motion. The flip amplitude is related to the viscosity and the shape of cation. By using the physicochemical parameters such as ionic conductivity, density, and viscosity, the experimental approaches were discussed for the classical SE, NE, and SED relations. We propose an empirical constant of SE for individual ions in ILs. Since ILs have specific properties induced by ion-ion interactions, deviations from classical relations are clearly shown. In this chapter, the experimental data are described following to the classical relationships without any modification to indicate the varieties of ILs. Particularly, cation diffusion in ionic liquids is shown to couple with a small-angle librational flip. Strong ion-ion interactions must be effective in various time-scales and distances in space. Theoretical approaches are waited to interpret the analysis based on the experimental data for ionic liquids.

8. Acknowledgements

The author expresses hearty thanks to Dr. Shiro Seki for the precise data of ionic conductivity, density and viscosity. She is also indebted to him and Drs. S. Tsuzuki, and Y. Umebayashi for their exciting discussion on the complex properties of the ILs.

9. References

[1] K. Hayamizu, S. Tsuzuki and S. Seki, *J. Phys. Chem.* A 112, 12027 (2008).
[2] K. Hayamizu, S. Tsuzuki, S. Seki, Y. Ohno, H. Miyashiro and Y. Kobayashi, *J. Phys. Chem.* B 112, 1189 (2008).
[3] K. Hayamizu, S. Tsuzuki, S. Seki, K. Fujii, M. Suenaga and Y. Umebayashi, *J. Chem. Phys.* 113, 194505 (2010).
[4] K. Hayamizu, S. Tsuzuki and S. Seki, and Y. Umebayashi, *J. Chem. Phys.* 135, 84505 (2011).
[5] W. S. Price, *NMR Studies of Translational Motion*, Cambridge University Press, Cambridge (2009).
[6] E. O. Stejskal and J. E. Tanner, *J. Chem. Phys.* 42, 288 (1965).
[7] J. E. Tanner, *J. Chem. Phys.* 52, 2523 (1970).
[8] D. D. Traficante, *Relaxation: An Introduction, in Encyclopedia of Nuclear Magnetic Resonance,* ed. M. D. Grant and R. K. Harris (Wiley, New York, 1996). Vol. 6, p. 3988.
[9] H. Antony, D. Mertens, A. Dölle, P. Wasserscheid and W. R. Carper, *ChemPhysChem.* 4, 588 (2003).
[10] W. R. Carper, P. G. Wahlbeck, J. H. Antony, D. Mertens, A. Dölle and P. Wasserscheid, *Anal. Bioanal. Chem.* 378, 1548 (2004).
[11] W. R. Carper, P. G. Wahlbeck and J. Dölle, *J. Phys. Chem.* A 108, 6096 (2004).
[12] J. H. Antony, A. Dölle, D. Mertens, P. Wasserscheid, W. R. Carper and P. G. Wahlbeck, *J. Phys. Chem.* A 109, 6676 (2005).
[13] N. E. Heimer, J. S. Wilkes, P. G. Wahlbeck and W. R. Carper, *J. Phys. Chem.* A 110, 868 (2008).

[14] M.Imanari, H. Tsuchiya, H. Seki, K. Nakanishi and M. Tashiro, *Magn. Reson. Chem.* 47, 67 (2009)
[15] M.Imanari, K. Uchida, K. Miyano, H. Seki and K. Nishikawa, *Phys. Chem. Chem. Phys.* 12, 2959 (2010).
[16] W. S. Price, K. Hayamizu, H. Ide, Y. Arata, *J. Magnetic Resonance,* 139, 205-212 (1999)
[17] R. Metzler and J. Klafter, *J. Physics Reports*, 2000, *339*, 1
[18] Y. Umebayashi, T. Fujimori, T. Sukizaki, M. Asada, K. Fujii, R. Kanzaki and S. Ishiguro, *J. Phys. Chem.* A 109, 8976 (2005).
[19] H. J. V. Tyrrell and K. R. Harris, Diffusion in Liquids: A Theoretical and Experimental Study (Butterworths, London, 1984).
[20] S. R. Becker, P. H. Poole and F. W. Starr, *Phys. Rev. Lett.* 97, 55901 (2006).
[21] A. Voronel, E. Veliyulin, V. S. Machavariani, A. Kisliuk and D. Quitmann, *Phys. Rev. Lett.* 80, 2630 (1988).
[22] K. R. Harris, *J. Chem. Phys.* 131, 054503 (2009).
[23] J. O'M. Bockris and A. K. N. Reddy, *Modern Electrochemistry*, Vol. 1, Plenum Press, New York (1998).
[24] W. Xu, E. I. Cooper and C. A. Angell, *J. Phys. Chem.* B 107, 6170 (2003).
[25] K. J. Fraser, E. I. Izgorodina, M. Forsyth, J. L. Scott and D. R. MacFarlane, *Chem. Commun.* 37, 3817 (2007).
[26] Y. Aihara, K. Sugimoto, W. S. Price and K. Hayamizu, *J. Chem. Phys.* 113, 1981 (2000).
[27] H. Tokuda, S. Tsuzuki, M. A. B. H. Susan, K. Hayamizu and M. Watanabe, *J. Phys. Chem*. B 110, 19593 (2006).
[28] 28 K. Ueno, H. Tokuda and M. Watanabe, *Phys. Chem. Chem. Phys.* 12, 1649 (2010) and references therein.
[29] R. Harris, *J. Phys. Chem.* B 114, 9572 (2010)
[30] Y. Umebayashi, T. Mitsugi, K. Fujii, S. Seki, K. Chiba, H. Yamamoto, J. N. C. Lopes, A. A. H. Pádua, M. Takeuchi, R. Kanzaki and S. Ishiguro, *J. Phys. Chem.* B 113, 4338 (2009).
[31] T. Fujimori, K. Fujii, R. Kanzaki, K. Chiba, H. Yamamoto, Y. Umebayashi and S. Ishiguro, *J. Mol. Liq.* 131–132, 216 (2007).
[32] A. Abragam, *The Principles of Nuclear Magnetism*, page 302 (Oxford, 1961).
[33] M. G. Mazza, N. Giovambattista, H. E. Stanley and F. W. Starr, *Phys. Rev.* E 76, 031203 (2007) and references therein.
[34] T. Köddermann, R. Ludwig and D. Paschek, *ChemPhysChem* 9, 1851 (2008).
[35] J. A. Ingram, R. S. Moog, N. Ito, R. Biswas and M. Maroncelli, *J. Phys. Chem.* B 107, 5926 (2003).
[36] Y. Yasaka, C. Wakai, N. Matubayasi and M. Nakahara, *J. Chem. Phys.* 127, 104506 (2007).
[37] H. Cang, J. Li and M. D. Fayer, *J. Chem. Phys.* 119, 13017 (2003).
[38] K. Dahl, G. M. Sando, D. M. Fox, T. E. Sutto and J. C. Owrutsky, *J. Chem. Phys.* 123, 84504 (2005).
[39] K. S. Mali, G. B. Dutt and T. Mukherjee, *J. Chem. Phys.* 128, 54504 (2008).
[40] N. E. Heimer, J. S. Wilkes, P. W. Wahlbeck and W. J. Carper, *J. Phys. Chem.* A 110, 868 (2006).
[41] A. Wulf, R. Ludwig, P. Sasisanker and H. Weingärtner, *Chem. Phys. Lett.* 439, 323 (2007).

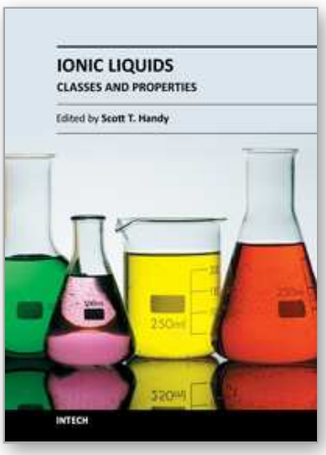

Ionic Liquids - Classes and Properties

Edited by Prof. Scott Handy

ISBN 978-953-307-634-8
Hard cover, 344 pages
Publisher InTech
Published online 10, October, 2011
Published in print edition October, 2011

Room temperature ionic liquids (RTILs) are an interesting and valuable family of compounds. Although they are all salts, their components can vary considerably, including imidazolium, pyridinium, ammonium, phosphonium, thiazolium, and triazolium cations. In general, these cations have been combined with weakly coordinating anions. Common examples include tetrafluoroborate, hexafluorophosphate, triflate, triflimide, and dicyanimide. The list of possible anionic components continues to grow at a rapid rate. Besides exploring new anionic and cation components, another active and important area of research is the determinination and prediction of their physical properties, particularly since their unusual and tunable properties are so often mentioned as being one of the key advantages of RTILs over conventional solvents. Despite impressive progress, much work remains before the true power of RTILs as designer solvents (i.e. predictable selection of a particular RTIL for any given application) can be effectively harnessed.

How to reference

In order to correctly reference this scholarly work, feel free to copy and paste the following:

Kikuko Hayamizu (2011). Translational and Rotational Motions for TFSA-Based Ionic Liquids Studied by NMR Spectroscopy, Ionic Liquids - Classes and Properties, Prof. Scott Handy (Ed.), ISBN: 978-953-307-634-8, InTech, Available from: http://www.intechopen.com/books/ionic-liquids-classes-and-properties/translational-and-rotational-motions-for-tfsa-based-ionic-liquids-studied-by-nmr-spectroscopy

INTECH
open science | open minds

InTech Europe
University Campus STeP Ri
Slavka Krautzeka 83/A
51000 Rijeka, Croatia
Phone: +385 (51) 770 447
Fax: +385 (51) 686 166
www.intechopen.com

InTech China
Unit 405, Office Block, Hotel Equatorial Shanghai
No.65, Yan An Road (West), Shanghai, 200040, China
中国上海市延安西路65号上海国际贵都大饭店办公楼405单元
Phone: +86-21-62489820
Fax: +86-21-62489821

IntechOpen